Temperature dependence of clumped isotopes ([?]47) in aragonite

Niels Jonathan de Winter[1], Rob Witbaard[2], Ilja Japhir Kocken[3], Inigo A Müller[4], Jingjing Guo[3], Barbara Goudsmit[2], and Martin Ziegler[3]

[1]Vrije Universiteit Brussel
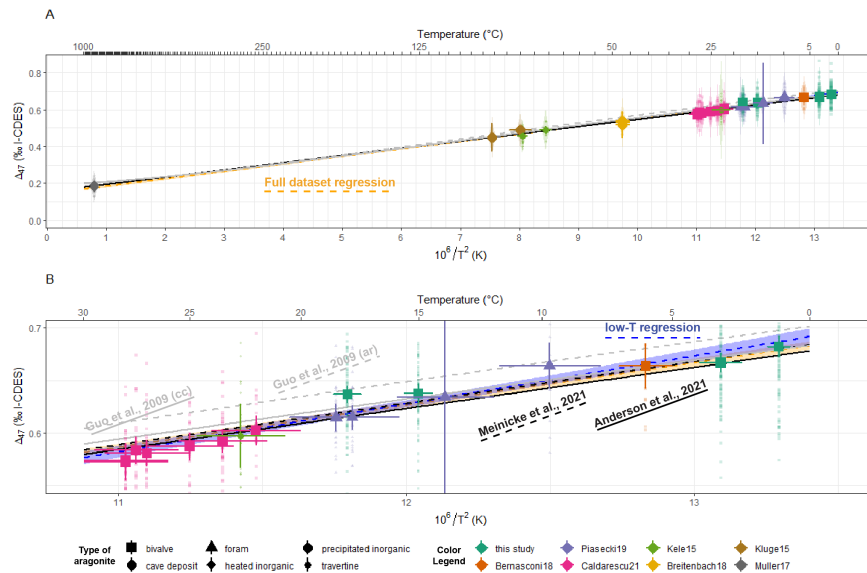[2]Royal Netherlands Institute for Sea Research
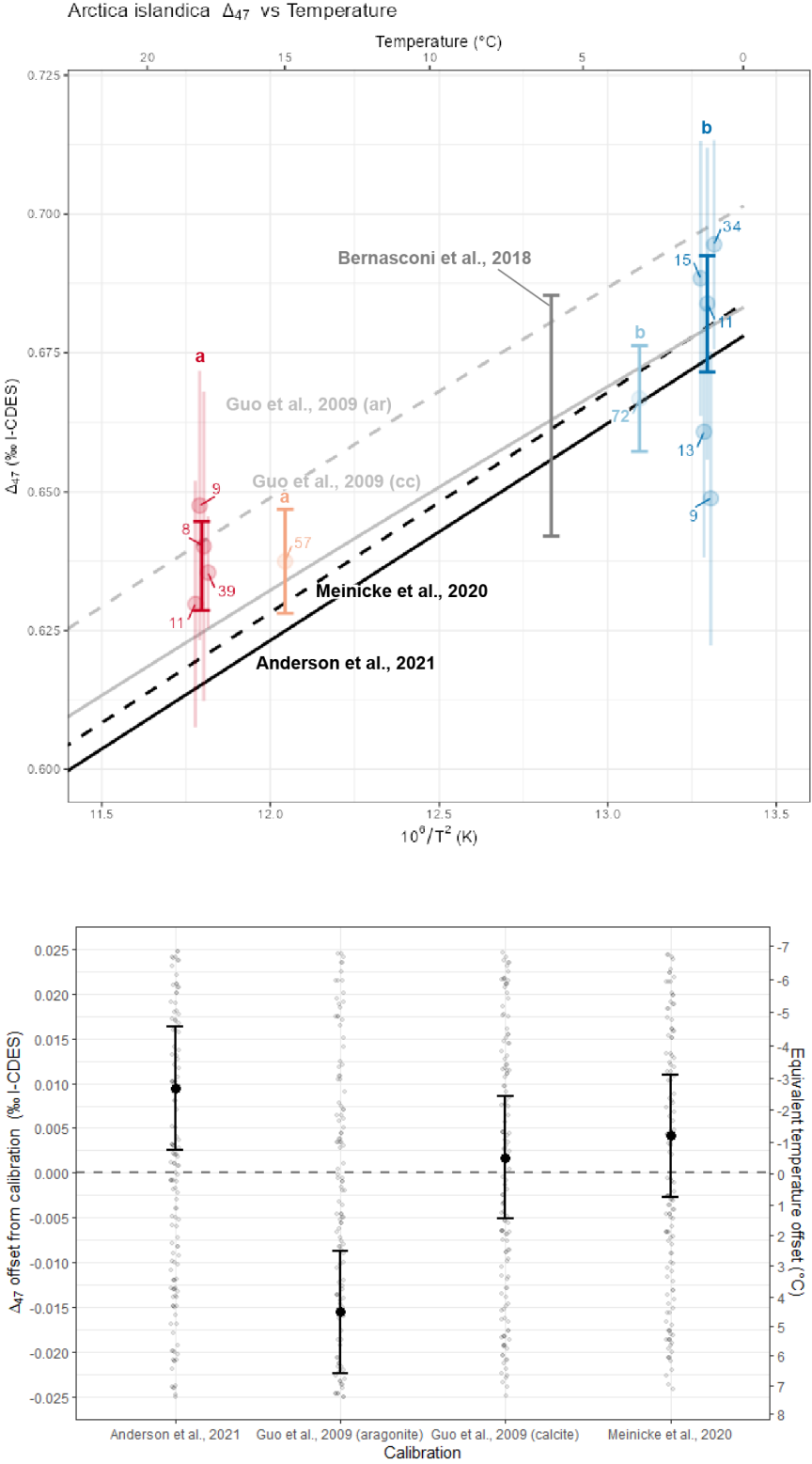[3]Utrecht University
[4]Université de Genève

November 30, 2022

Abstract

Clumped isotope thermometry can independently constrain the formation temperatures of carbonates, but a lack of precisely temperature-controlled calibration samples limits its application on aragonites. To address this issue, we present clumped isotope compositions of aragonitic bivalve shells grown under highly controlled temperatures (1-18°C), which we combine with clumped isotope data from natural and synthetic aragonites from a wide range of temperatures (1-850degC). We observe no discernible offset in clumped isotope values between aragonitic foraminifera, mollusks, and abiogenic aragonites or between aragonites and calcites, eliminating the need for a mineral-specific calibration or acid fractionation factor. However, due to non-linear behavior of the clumped isotope thermometer, including high-temperature (>100degC) datapoints in linear clumped isotope calibrations causes them to underestimate temperatures of cold (1-18degC) carbonates by 2.7 +- 2.0degC (95% confidence level). Therefore, clumped isotope-based paleoclimate reconstructions should be calibrated using samples with well constrained formation temperatures close to those of the samples.

Arctica islandica Δ_{47} vs Temperature

1   **Temperature dependence of clumped isotopes (Δ_{47}) in aragonite**

2   Niels J. de Winter[1,2], Rob Witbaard[3], Ilja J. Kocken[2], Inigo A. Müller[4], Jingjing Guo[2], Barbara

3   Goudsmit[2,3], Martin Ziegler[2]

4

5   [1]Analytical, Environmental and Geochemistry Group, Vrije Universiteit Brussel, Belgium

6   [2]Dept. of Earth Sciences, Utrecht University, the Netherlands

7   [3]Dept. of Estuarine and Delta Systems, Royal Netherlands Institute for Sea Research, the

8   Netherlands.

9   [4]Department of Earth Science, University of Geneva, Switzerland

10

Key points

- Precise control on carbonate formation temperatures enables more accurate clumped isotope-temperature calibrations
- Isotopic ordering and acid fractionation in aragonite have a similar temperature dependence as in calcite, enabling combined calibrations
- The Δ_{47}-$\frac{1}{T^2}$ relation in carbonates is non-linear, including hot calibration data offsets the calibration in the cold temperature range

Abstract

Clumped isotope thermometry can independently constrain the formation temperatures of carbonates, but a lack of precisely temperature-controlled calibration samples limits its application on aragonites. To address this issue, we present clumped isotope compositions of aragonitic bivalve shells grown under highly controlled temperatures (1–18°C), which we combine with clumped isotope data from natural and synthetic aragonites from a wide range of temperatures (1–850°C). We observe no discernible offset in clumped isotope values between aragonitic foraminifera, mollusks, and abiogenic aragonites or between aragonites and calcites, eliminating the need for a mineral-specific calibration or acid fractionation factor. However, due to non-linear behavior of the clumped isotope thermometer, including high-temperature (>100°C) datapoints in linear clumped isotope calibrations causes them to underestimate temperatures of cold (1–18°C) carbonates by 2.7 ± 2.0°C (95% confidence level). Therefore, clumped isotope-based paleoclimate reconstructions should be calibrated using samples with well constrained formation temperatures close to those of the samples.

Plain language summary

35   Clumped isotope analysis is a highly accurate method for reconstructing temperatures in

36   Earth's past climate from calcium carbonate fossils of calcifying organisms. Unfortunately,

37   calibration studies so far were predominantly based on samples of calcite, a common calcium

38   carbonate mineral. It is therefore unknown whether these clumped isotope calibrations yield

39   accurate temperature reconstructions when applied to aragonite, another carbonate mineral

40   which corals and many shells consist of. Therefore, we grew mollusks that build their shell out

41   of aragonite in a lab at constant water temperatures to test the clumped isotope method on

42   aragonitic shells. We find no significant difference in the temperature sensitivity of the method

43   between our aragonites and the previous calibrations and show that the temperature

44   calibration can be improved by combining data from different minerals. However, we find subtle

45   differences in the temperature dependence of clumped isotopes between hot (>100°C)

46   carbonates and cold (<30°C) carbonates, which cause previous calibrations to underestimate

47   temperatures of colder carbonates. We conclude that using carbonate samples grown at

48   temperatures close to the temperatures of the samples used in climate reconstructions can

49   eliminate a bias of 2.7°C, resulting in more accurate reconstructions of past temperatures.

50

53

54   **1. Introduction**

55   Since its first applications (e.g. Schauble et al., 2003; Wang et al., 2004; Ghosh et al., 2006),

56   carbonate clumped isotope analysis has developed into a valuable tool for paleothermometry

57   in the geosciences. Clumped isotope analysis is based on the thermodynamic principle that

58   molecules with multiple heavy isotopes (so-called "multiply-substituted isotopologues") have

59   lower vibrational energies than molecules containing lighter isotopes (Urey, 1947).

60   Consequently, the increase in system entropy at higher temperatures causes a decrease in

61   the occurrence of multiply-substituted isotopologues, and "clumping" of heavy isotopes within

62   the same molecule is favored in low-energy systems (Eiler, 2007). In carbonates, this principle

63   causes heavy carbonate ions (e.g. $^{13}C^{18}O^{16}O_2$; mass 63 or $^{12}C^{18}O_2^{16}O$; mass 64) to become

64   more abundant with decreasing calcification temperatures (Ghosh et al., 2006). The

65   distribution of these isotopologues is proportional in the CO_2 gas after reaction of carbonates

66   with acid (e.g. $^{13}C^{18}O^{16}O$; mass 47 and $^{12}C^{18}O_2$, mass 48 respectively) and is measured with

67   reference to the distribution of isotopologues in a fully scrambled heated CO_2 gas with the

68   same isotopic composition:

69
$$\Delta_{47}[‰] = \left(\frac{R^{47}}{R^{47}*} - 1\right) \quad (1)$$

70   In which R^{47} is the ratio of CO_2 molecules with mass 47 (predominantly $^{13}C^{18}O^{16}O$) relative to

71   CO_2 with the most common mass 44 ($^{12}C^{16}O_2$) in the sample, and R^{47*} is the same ratio in

72   stochastic equilibrium (Daëron et al., 2016). This Δ_{47} value is a measure for the degree of

73   "clumping" in the sample which depends on its calcification temperature.

74   The main advantage of carbonate clumped isotope analysis over previous paleothermometers

75   is its basis on thermodynamic principles and its independence from the chemistry of the

76   precipitation fluid (Eiler, 2007). The latter represents an improvement over the often-used

77   oxygen isotope paleothermometer ($\delta^{18}O$), which requires knowledge of the oxygen isotope

78   composition of the precipitation fluid ($\delta^{18}O_w$; e.g. Epstein et al., 1953; Kim & O'Neil, 1997). The

79   clumped isotope method has many applications, notably to reconstruct absolute temperature

80   variability throughout Earth's history (Rodríguez-Sanz et al., 2017; Henkes et al., 2018; Vickers

81   et al., 2020a; de Winter et al., 2021a; Meckler et al., 2022; Agterhuis et al., 2022).

82   Inter-lab standardization of carbonate Δ_{47} measurements has reconciled former offsets

83   between laboratories using different CO_2 preparation methods and reconciled the clumped

84   isotope temperature calibration of calcites with the results of thermodynamic *ab initio* models

85   (Bernasconi et al., 2018; 2021; Petersen et al., 2019; Jautzy et al., 2020). A unified linear

86   calibration was established through re-standardized Δ_{47} values of carbonates precipitated at a

87   wide range of known temperatures (0.5-1100°C; Anderson et al., 2021). This eliminates

88   concerns over the confounding effects of differences in the origin of carbonates (e.g. biogenic

89   vs. inorganic; Henkes et al., 2013), varying mineralization rates (Daëron et al., 2019), different

90   acid digestion temperatures and different carbonate mineralogies (e.g. dolomite vs. calcite;

91   Müller et al., 2019) on the clumped isotope thermometer. However, it remains unclear whether

92   biological process (i.e. "vital effects") influence isotopic ordering in some biogenic carbonates.

93   The unified calibration dataset includes only one aragonitic carbonate, insufficient to test for

94   different clumped isotope temperature dependencies between aragonites and calcites

95   (Anderson et al., 2021). Results of *ab initio* models suggest that such a difference between the

96   two polymorphs may exist (Schauble et al., 2006; Guo et al., 2009) and experimental studies

97   disagree on a difference in acid fractionation factor (AFF) between calcite and aragonite (Guo

98   et al., 2009; Müller et al., 2019; Petersen et al., 2019). These uncertainties are confounded by

99   the fact that most carbonates used in current calibrations are precipitated under natural

100   circumstances with indirectly estimated or else poorly controlled temperature regimes (e.g.

101   Kele et al., 2015; Peral et al., 2018). The potential Δ_{47} offset between aragonite and calcite

102   might introduce an unknown bias when using the unified temperature calibration on aragonite

103   data (e.g. Caldarescu et al., 2021); a severe limitation given the common occurrence of

104   aragonite in biogenic calcifiers (e.g. bivalves; Kennedy et al., 1969, gastropods; Taylor and

105   Reid, 1990, and foraminifera; Hansen, 1979) as well as inorganic natural carbonates (e.g.

106   speleothems; Frisia et al., 2000, and travertines; Kele et al., 2015).

107   This study presents new clumped isotope results from precisely temperature controlled, lab-

108   grown aragonitic *Arctica islandica* bivalve shells. The bivalve *Arctica islandica* is a highly

109   utilized climate archive, and a promising substrate for clumped isotope-based

110   paleothermometry (e.g. Witbaard et al., 1997; Burchardt and Simonarson, 2003; Schöne et al.,

111   2005; Schöne and Fiebig, 2009; Butler et al., 2013). Combined with preexisting aragonite

112   clumped isotope data (Kluge et al., 2015; Kele et al., 2015; Müller et al., 2017; Breitenbach et

113   al., 2018; Bernasconi et al., 2018; Piasecki et al., 2019; Caldarescu et al., 2021) standardized

to the new Intercarb-Carbon Dioxide Equilibrium Scale (I-CDES) reference frame (Bernasconi et al., 2021), our dataset resolves potential vital effects on clumped isotopes in aragonitic mollusks by comparing species and specimens grown under the same controlled conditions. This study aims to offer a detailed investigation of the clumped isotope temperature dependence in aragonites.

2. Materials and Methods

2.1 Lab grown Arctica islandica

Arctica islandica bivalves were cultured inside the lab of the Royal Netherlands Institute for Sea Research (NIOZ, Texel, the Netherlands). Specimens used for this study were grown under four different, constant, and monitored temperature regimes: 1.1 ± 0.2°C, 3.2 ± 0.3°C, 15 ± 0.4°C and 18 ± 0.3°C (see **Table 1**; **S9**). Details on the culturing setup are provided in **S1** and Witbaard et al. (1998). Aragonite from cleaned and dried *Arctica islandica* shells was sampled using a hand-held Dremel 3000 rotary drill at low speed equipped with a tungsten-carbide drill bit (see **S1**). Gathering enough aragonite for reliable Δ_{47} analyses for each temperature treatment (>2 mg; Müller et al., 2017; Fernandez et al., 2017) typically required combining material from multiple (3–5) specimens grown under the same temperature conditions. To test potential inter-specimen differences, results were tracked per individual specimen for the 1.1 ± 0.2°C and 18 ± 0.3°C treatments (see **Table 1**).

2.2 Clumped isotope analysis

The clumped isotope composition of 278 aliquots of shell aragonite were analyzed over two 6-month periods (March – August 2020; May – November 2021) on two Thermo isotope ratio mass spectrometers (one MAT253 and one MAT253 plus) coupled to Kiel IV carbonate preparation devices (see **S1**). After correcting for variability in the pressure baseline (He et al.,2012), clumped isotope results were processed relative to the I-CDES through an empirical transfer function (ETF) based on measurements of ETH standards (ETH-1, -2 and -3) and their

140   accepted I-CDES values (Bernasconi et al., 2021). Isotopic values were calculated using the

141   latest IUPAC values (Brand et al., 2010; Daëron et al., 2016). No AFF was applied after I-

142   CDES standardization because the carbonate standards used for the ETF undergo the same

143   acid reaction as the samples (Bernasconi et al., 2021). Long-term accuracy and reproducibility

144   of Δ_{47} results were assessed based on repeated measurements of the IAEA-C2 monitoring

145   standard (Δ_{47_IAEA} on MAT253 plus: 0.6382 ± 0.026‰; Δ_{47_IAEA} on MAT253: 0.6445 ± 0.046‰;

146   1σ). Results were indistinguishable from the accepted value for IAEA-C2 (0.6409 ± 0.003‰;

147   95% CL; Bernasconi et al., 2021). Full results of all sample aliquots and standards used to

148   standardize the results are provided in **S2**.

149   *2.3 Data compilation*

150   The *Arctica islandica* dataset was augmented with literature Δ_{47} values of aragonites with

151   known calcification temperatures (see **S3**). The dataset includes samples from mollusks

152   (Bernasconi et al., 2018; aragonitic *Megapitaria aurantiaca* samples in Caldarescu et al., 2021;

153   this study), foraminifera (Piasecki et al., 2019), travertines (Kele et al., 2015; Bernasconi et al.,

154   2018), cave deposits (Breitenbach et al., 2018), lab-grown aragonites (Kluge et al., 2015) and

155   heated aragonites (Müller et al., 2017). Data from several older studies (e.g. Ghosh et al.,

156   2006; 2007; Tripati et al., 2010; Wacker et al., 2013; 2014; Zhang et al., 2018; Zhai et al., 2019;

157   Dong et al., 2021) were not included because they were not corrected for the pressure baseline

158   (He et al., 2012; Bernasconi et al., 2013), could not be transferred into the standard reference

159   frame (Dennis et al., 2011), lacked the standardization required to bring Δ_{47} values into the I-

160   CDES scale (Bernasconi et al., 2021) or because the aragonite was precipitated out of

161   equilibrium (e.g. Kimball et al., 2015; Chen et al., 2019; **S1**; **S3**). Clumped isotope data from

162   the literature was brought to the I-CDES reference frame using the multi-linear correction

163   proposed in Appendix A of Bernasconi et al. (2021) using values of carbonate standards

164   reported in the studies (see **S1**). Uncertainties on the formation temperatures of the non-

165   temperature controlled datapoints from previous studies were generally in the order of 1°C (1σ;

166   see **S1**). The full dataset including Δ_{47} values and temperatures with their uncertainties used

167   in this study is provided in **S4**. Unless stated otherwise, uncertainties are cited at the 95%

168   confidence level.

169   All data processing for this study is done in R (R Core Team, 2022) and scripts are provided

170   in **S5** and published on Github (https://github.com/nielsjdewinter/Aragonite_clumped). Details

171   on data processing are provided in **S1**. We compare our data with calibrations by Anderson et

172   al. (2021) and Meinicke et al. (2020) as well as with temperature dependencies of aragonite

173   and calcite clumped isotope compositions from *ab initio* modelling in Guo et al. (2009) brought

174   into the I-CDES reference frame (see **S1**).

3. Results

3.1 Clumped isotope values in Arctica islandica

Clumped isotope results from *A. islandica* are summarized in **Table 1** and **Figure 1**. There is no significant clumped isotope difference between specimens in the same temperature treatment ($F_{(4,77)} = 1.937$, $p = 0.11$ for the 1°C specimens and $F_{(3,63)} = 0.377$, $p = 0.77$ for the 18°C specimens; see **S6**). The number of measurements per specimen was large enough to exclude per-specimen Δ_{47} differences outside the reproducibility standard deviation of the clumped isotope analyses (0.046‰; see **Table 1** and **S6**). Differences between all temperature treatments are statistically significant ($P_{(3,274)} = 15.68$, $p < 0.01$), except for differences between the 15°C and 18°C temperature bin and the difference between 1°C and 3°C (95%CL; **S6**).

We investigated the Δ_{47}-$\frac{1}{T^2}$ relationship and how it varies along the temperature domain by performing linear regressions on increasingly large parts of our compilation. Note that the uncertainty on clumped isotope data compared to the range of temperatures of the lab-grown *A. islandica* leaves relatively high uncertainty on a clumped isotope-temperature regression through these results alone compared to the unified clumped isotope calibration (Anderson et al. 2021). We therefore do not advice using this and other regression equations in this section for calibrating clumped isotope results (see **Discussion**). Firstly, a statistically significant temperature relationship (Δ_{47}-$\frac{1}{T^2}$ slope >0; 95% CL) is found for Δ_{47} exclusively from *Arctica islandica* samples:

$$\Delta_{47}(I-CDES) = 0.0280 \pm 0.0042 * \frac{10^6}{T^2} + 0.304 \pm 0.0524 \text{ (T in K, } \pm 1\sigma; \sigma_{res} = 0.047‰)} \qquad (1)$$

Secondly, including other aragonitic mollusk data (Caldarescu et al., 2021) yields a regression indistinguishable from the Anderson et al. (2021) unified clumped isotope calibration:

$$\Delta_{47}(I-CDES) = 0.0443 \pm 0.0024 * \frac{10^6}{T^2} + 0.097 \pm 0.0291 \text{ (T in K, } \pm 1\sigma; \sigma_{res} = 0.043‰)} \qquad (2)$$

197

3.2 Aragonite clumped isotope temperature dependence

When including clumped isotope values of other low-temperature (<30°C) aragonites in the compilation, the regression remains indistinguishable from the calibration of Anderson et al. (2021) and similar to Meinicke et al. (2020; 2021) and the Guo et al. (2009) theoretical temperature relationships (**Fig. 2B**):

$$\Delta_{47}(I-CDES) = 0.0451 \pm 0.0024 * \frac{10^6}{T^2} + 0.0871 \pm 0.0287 \text{ (T in K}, \pm 1\sigma; \sigma_{res} = 0.042‰)} \qquad (3)$$

Finally, we included higher temperature (>30°C) datapoints, such as the cave deposits of Breitenbach et al. (2018), travertine samples from Kele et al. (2015), precipitated aragonites from Kluge et al. (2015) and heated aragonites from Müller et al. (2017) in the linear regression. This decreases the slope and increases the intercept (see **Fig. 2**):

$$\Delta_{47}(I-CDES) = 0.0403 \pm 0.0005 * \frac{10^6}{T^2} + 0.1435 \pm 0.0485 \text{ (T in K}, \pm 1\sigma; \sigma_{res} = 0.040‰)} \qquad (4)$$

The formation temperatures of our *A. islandica* data on the very cold end of the calibration domain are significantly underestimated by Anderson et al. (2021; $\Delta\Delta_{47}$ = +0.009 ± 0.007‰; −2.71 ± 2.03°C; **Fig. 3**; $\Delta\Delta_{47}$ = offset between data and calibration). The theoretical aragonite clumped isotope-temperature relationship (Guo et al., 2009) severely overestimates *A. islandica* temperatures (−0.016 ± 0.007‰; +4.35 ± 1.88°C; **Fig. 3**). Contrarily, the Meinicke et al. (2020; 2021) calibration ($\Delta\Delta_{47}$ = +0.004 ± 0.007‰; −1.17 ± 2.00°C; **Fig. 3**) and the theoretical calcite temperature relationship (Guo et al., 2009; $\Delta\Delta_{47}$ = +0.002 ± 0.007‰; −0.47 ± 1.98°C; **Fig. 4**) do not significantly over- or underestimate the formation temperature of our *A. islandica* shells.

4. Discussion

4.1 Isotope ordering in aragonitic mollusks

218 Clumped isotope values of our temperature-controlled *A. islandica* samples consistently plot

219 on a Δ_{47}-$\frac{1}{T^2}$ linear relationship with other low-temperature aragonite datapoints (**Fig. 1 and 2**;

220 see **section 4.2**). The absence of a consistent offset between *A. islandica* datapoints and other

221 aragonites (mean Δ_{47} difference of +0.003 ± 0.004‰, see **Fig. 2** and **S8**) and agreement

222 between the linear Δ_{47}-$\frac{1}{T^2}$ dependence of the aragonitic mollusk data in this study and the

223 regression through the complete low-temperature aragonite dataset (**Fig. 1** and **section 3.1**)

224 strongly supports a common temperature dependence for all aragonites in this study, biogenic

225 or inorganic, and argues against disequilibrium fractionation in aragonite precipitated

226 inorganically or vital effect in bivalves or foraminifera (see **section 3.1**; **Fig. 1 and 2**). Our

227 highly temperature-controlled growth experiments uniquely allow us to exclude variability in

228 the growth environment between specimens from the same growth treatment as a driver of

229 shell composition. Strong similarity of Δ_{47} values between individual *A. islandica* specimens

230 grown at the same temperature thus rules out specimen-specific vital effects on the clumped

231 isotope composition aragonitic bivalve shells outside the uncertainty of our measurements (see

232 **section 3.1**; **Fig. 1**, **Table 1** and **S6**). These findings corroborate measurements in calcitic

233 mollusks showing that clumped isotope values in mollusk carbonates adhere to the same

234 temperature relationship as other carbonates precipitated in equilibrium (except for juvenile

235 oyster shells; Huyghe et al., 2022). Clumped isotope analyses in (fossil) mollusk shells thus

236 provide an independent temperature proxy, allowing paleoclimatologists to disentangle the

237 effects of variability in temperature and the hydrological cycle (as measured in $\delta^{18}O_w$)

238 throughout geological history down to the seasonal timescale (e.g. Caldarescu et al., 2021; de

239 Winter et al., 2021; Letulle et al., 2022).

240 *4.2 Mineral-specific acid fractionation factor*

241 Residuals of aragonite clumped isotope data around the low-temperature (<30°C) York

242 regression (0.042‰; 1σ; see **section 3.**1 and **Fig. 2**) are predominantly explained by analytical

243 uncertainty on Δ_{47} measurements (external precision of 0.026‰ and 0.046‰ on the 253Plus

244 and the MAT253 mass spectrometers; 1σ; see **section 2.2**). Uncertainty on formation

245   temperatures in the low-temperature dataset (±0.8°C; 1σ; see **S4**) would add an additional

246   uncertainty of 0.0024‰ (1σ) if applied to the weighted average formation temperature of all

247   low-temperature (<30°C) data points (22.0°C; see **S4**). Outside these uncertainties in the

248   compilation data, there is little uncertainty on the temperature relationship in the low-

249   temperature domain (<30°C; see **section 3.2**; **Fig. 2**). If clumped isotope fractionation during

250   acid digestion was indeed different between aragonite and calcite (as suggested in Müller et

251   al., 2017; Petersen et al., 2019) the difference in AFF would be indicated by the difference

252   between our aragonite dataset and the previous calcite-based calibrations (Meinicke et al.,

253   2020; 2021). The close similarity between our *A. islandica* data and the calcite calibration ($\Delta\Delta_{47}$

254   = 0.004 ± 0.007‰; **Fig. 3**; **S7**) leaves little room for the 0.007‰ and 0.025‰ difference in AFF

255   reported in Petersen et al. (2019) and Müller et al. (2017), respectively. We therefore conclude

256   that the calcite AFF in Petersen et al. (2019), which are included in the I-CDES reference scale

257   (Bernasconi et al., 2021) can be used for aragonite samples.

258   *4.3 Non-linear temperature dependence of clumped isotopes in aragonites*

259   Current clumped isotope calibrations (Meinicke et al., 2020; 2021; Anderson et al., 2021) show

260   subtle differences in the low-temperature end of the calibration (<30°C) that would result in

261   ~1.5°C colder temperatures when applying Anderson et al. (2021) compared to Meinicke et al.

262   (2020). In addition, the cold-water (<30°C) carbonate based Meinicke et al. (2020) calibration

263   more closely resembles the modelled temperature relationship for calcites in Guo et al. (2009).

264   Including high-temperature (>30°C) data in our linear regression leads to overestimation of the

265   temperature of warmer (>18°C) datapoints ($\Delta\Delta_{47}$ of -0.005 ± 0.006‰, or $+1.8^{+2.1}_{-2.0}$°C for data

266   precipitated at 30°C), while underestimating colder datapoints ($\Delta\Delta_{47}$ of +0.009 ± 0.008‰, or

267    $-2.0^{+2.0}_{-2.0}$°C for data precipitated at 0°C; **Fig. 2**; **S7**). Point-by-point offsets of all data from the

268   calibration lines are provided in **S8**.

269   This difference between Δ_{47}-$\frac{1}{T^2}$ regressions through the low-temperature (<30°C) and the full

270   dataset (see **section 3.2**; **Fig 2**) likely highlights non-linear behavior of the Δ_{47}-$\frac{1}{T^2}$ relationship

271   in aragonites. In fact, previous studies based on both clumped isotope analyses and *ab initio*

272   modelling have suggested a non-linear Δ_{47}-$\frac{1}{T^2}$ relationship to be a better fit for both calcites

273   (Guo et al., 2009; Jautzy et al., 2020) and dolomites (Guo et al., 2009; Müller et al., 2019)

274   precipitated on a large range of known temperatures. Non-linear behavior is also observed in

275   the Anderson et al. (2021) dataset, where Δ_{47} values of calcites precipitated between 100°C

276   and 1000°C are underestimated by the linear relationship, while the hottest datapoints (calcites

277   heated to 1100°C) fall on the linear regression, mimicking the reduced Δ_{47}-$\frac{1}{T^2}$ slope at the high

278   temperature end of the polynomial regressions through calcite and dolomite data (Guo et al.,

279   2009; Jautzy et al., 2020; Müller et al., 2019). A linear Δ_{47}-$\frac{1}{T^2}$ relationship through a calibration

280   dataset with a large temperature range will thus overestimate temperatures for samples with

281   Δ_{47} values between 0.2‰ and 0.4‰ (temperatures of 100°C–1000°C; see residuals in

282   Anderson et al., 2021) and underestimate temperatures of cold (<30°C) samples, as confirmed

283   by regressions through our low-temperature datapoints (see **Fig. 2-3** and **section 4.4**).

284   Therefore, more high-temperature aragonite datapoints are needed to constrain the clumped

285   isotope-temperature relationship for temperatures >100°C.

286   *4.4 Calibrating the clumped isotope-temperature relationship in cold (<30°C) carbonates*

287   Our lab-grown *A. islandica* shells offer more control on formation temperature than naturally

288   grown carbonates precipitated under variable temperatures. Ideally, the temperature of these

289   natural samples is monitored so an average temperature can be calculated for the targeted

290   growth period (e.g. Kele et al., 2015; de Winter et al., 2020; 2021b; Huyghe et al., 2021).

291   However, formation temperatures are often indirectly estimated through other proxies (e.g.

292   $\delta^{18}O_c$) and/or estimates of the living environment (e.g. water depth) of the carbonate producer,

293   accumulating uncertainty (e.g. Peral et al., 2018; Piasecki et al., 2018; Meinicke et al., 2020).

294   These caveats obscure the full uncertainty of the formation temperatures of natural carbonates

295   as well as the effect of this unknown uncertainty on the calibrations. Considering the methods

296   by which the "known" temperatures of natural carbonates are estimated in previous studies,

part of the ~1.5°C temperature offset between Anderson et al. (2021) and Meinicke et al. (2020; 2021; see **Fig. 3**) and the 2.7 ± 2.0°C offset between Anderson et al. (2021) and our *A. islandica* data might be caused by uncertainty on the formation temperatures of the calibration dataset. However, our highly temperature-controlled *A. islandica* datapoints reveal that, despite uncertainty on formation temperature, the Meinicke et al. (2021) calibration locally approximates the non-linear Δ_{47}-$\frac{1}{T^2}$ relationship in the cold temperature domain with higher accuracy than the Anderson et al. (2021) calibration (**Fig. 1**, **Fig. 3**; **S8**). The non-linear theoretical calcite temperature dependence by Guo et al. (2009) also fits well with the data. Precisely temperature-controlled carbonates thus better constrain the slope of the Δ_{47}-$\frac{1}{T^2}$ relationship for cold carbonates (improving calibration accuracy) while reducing the uncertainty on the calibration (improving calibration precision).

The ~1.5°C difference in reconstructed temperature between the calibrations in the low temperature range (<30°C) may seem trivial and requires the complete *A. islandica* dataset (N = 278; see **Fig. 4**) to resolve. However, in paleoclimate reconstructions (e.g. Petersen et al., 2016; de Winter et al., 2017; 2021a; Vickers et al., 2020b; Agterhuis et al., 2021; Meckler et al., 2022), this temperature offset may have significant consequences. A ~1.5°C cold bias in temperature reconstructions may lead to a significant underestimation of climate sensitivity to CO_2 forcing, biasing the physical science basis for informing policymakers about future climate change (e.g. Dennis et al., 2013; Modestou et al., 2020; Westerhold et al., 2020; Tierney et al., 2020; IPCC, 2021). Accurate clumped isotope-based temperature reconstructions therefore require calibration datasets with precisely constrained formation temperatures tailored to the temperature range of the samples.

328

329 **Open Research**

330 Supplementary materials are deposited on the open-source repository Zenodo and can be

331 accessed through the following link: https://doi.org/10.5281/zenodo.6524705. R scripts are

332 uploaded on GitHub (https://github.com/nielsjdewinter/Aragonite_clumped) and archived in

333 Zenodo (https://doi.org/10.5281/zenodo.6560188).

References

Agterhuis, T., Ziegler, M., de Winter, N. J., and Lourens, L. J.: Warm deep-sea temperatures across Eocene Thermal Maximum 2 from clumped isotope thermometry, Commun Earth Environ, 3, 1–9, https://doi.org/10.1038/s43247-022-00350-8, 2022.

Anderson, N. T., Kelson, J. R., Kele, S., Daëron, M., Bonifacie, M., Horita, J., Mackey, T. J., John, C. M., Kluge, T., Petschnig, P., Jost, A. B., Huntington, K. W., Bernasconi, S. M., and Bergmann, K. D.: A Unified Clumped Isotope Thermometer Calibration (0.5–1,100°C) Using Carbonate-Based Standardization, 48, e2020GL092069, https://doi.org/10.1029/2020GL092069, 2021.

Bajnai, D., Guo, W., Spötl, C., Coplen, T. B., Methner, K., Löffler, N., Krsnik, E., Gischler, E., Hansen, M., Henkel, D., Price, G. D., Raddatz, J., Scholz, D., and Fiebig, J.: Dual clumped isotope thermometry resolves kinetic biases in carbonate formation temperatures, Nat Commun, 11, 4005, https://doi.org/10.1038/s41467-020-17501-0, 2020.

Bernasconi, S. M., Hu, B., Wacker, U., Fiebig, J., Breitenbach, S. F., and Rutz, T.: Background effects on Faraday collectors in gas-source mass spectrometry and implications for clumped isotope measurements, 27, 603–612, 2013.

Bernasconi, S. M., Müller, I. A., Bergmann, K. D., Breitenbach, S. F., Fernandez, A., Hodell, D. A., Jaggi, M., Meckler, A. N., Millan, I., and Ziegler, M.: Reducing uncertainties in carbonate clumped isotope analysis through consistent carbonate-based standardization, 19, 2895–2914, 2018.

Bernasconi, S. M., Daëron, M., Bergmann, K. D., Bonifacie, M., Meckler, A. N., Affek, H. P., Anderson, N., Bajnai, D., Barkan, E., Beverly, E., Blamart, D., Burgener, L., Calmels, D., Chaduteau, C., Clog, M., Davidheiser-Kroll, B., Davies, A., Dux, F., Eiler, J., Elliott, B., Fetrow, A. C., Fiebig, J., Goldberg, S., Hermoso, M., Huntington, K. W., Hyland, E., Ingalls, M., Jaggi, M., John, C. M., Jost, A. B., Katz, S., Kelson, J., Kluge, T., Kocken, I. J., Laskar, A., Leutert, T. J., Liang, D., Lucarelli, J., Mackey, T. J., Mangenot, X., Meinicke, N., Modestou, S. E., Müller, I. A., Murray, S., Neary, A., Packard, N., Passey, B. H., Pelletier, E., Petersen, S., Piasecki, A., Schauer, A., Snell, K. E., Swart, P. K., Tripati, A., Upadhyay, D., Vennemann, T., Winkelstern, I., Yarian, D., Yoshida, N., Zhang, N., and Ziegler, M.: InterCarb: A Community Effort to Improve Interlaboratory Standardization of the Carbonate Clumped Isotope Thermometer Using Carbonate Standards, 22, e2020GC009588, https://doi.org/10.1029/2020GC009588, 2021.

Breitenbach, S. F. M., Mleneck-Vautravers, M. J., Grauel, A.-L., Lo, L., Bernasconi, S. M., Müller, I. A., Rolfe, J., Gázquez, F., Greaves, M., and Hodell, D. A.: Coupled Mg/Ca and clumped isotope analyses of foraminifera provide consistent water temperatures, Geochimica et Cosmochimica Acta, 236, 283–296, https://doi.org/10.1016/j.gca.2018.03.010, 2018.

Buchardt, B. and Símonarson, L. A.: Isotope palaeotemperatures from the Tjörnes beds in Iceland: evidence of Pliocene cooling, Palaeogeography, Palaeoclimatology, Palaeoecology, 189, 71–95, https://doi.org/10.1016/S0031-0182(02)00594-1, 2003.

Butler, P. G., Wanamaker, A. D., Scourse, J. D., Richardson, C. A., and Reynolds, D. J.: Variability of marine climate on the North Icelandic Shelf in a 1357-year proxy archive based on growth increments in the bivalve Arctica islandica, 373, 141–151, 2013.

Caldarescu, D. E., Sadatzki, H., Andersson, C., Schäfer, P., Fortunato, H., and Meckler, A. N.: Clumped isotope thermometry in bivalve shells: A tool for reconstructing seasonal upwelling, Geochimica et Cosmochimica Acta, 294, 174–191, https://doi.org/10.1016/j.gca.2020.11.019, 2021.

Chen, S., Ryb, U., Piasecki, A. M., Lloyd, M. K., Baker, M. B., and Eiler, J. M.: Mechanism of solid-state clumped isotope reordering in carbonate minerals from aragonite heating experiments, Geochimica et Cosmochimica Acta, 258, 156–173, https://doi.org/10.1016/j.gca.2019.05.018, 2019.

380   Daëron, M., Blamart, D., Peral, M., and Affek, H. P.: Absolute isotopic abundance ratios and the
381   accuracy of Δ47 measurements, 442, 83–96, 2016.

382   Daëron, M., Drysdale, R. N., Peral, M., Huyghe, D., Blamart, D., Coplen, T. B., Lartaud, F., and
383   Zanchetta, G.: Most Earth-surface calcites precipitate out of isotopic equilibrium, 10, 429,
384   https://doi.org/10.1038/s41467-019-08336-5, 2019.

385   De Winter, N., Vellekoop, J., Vorsselmans, R., Golreihan, A., Soete, J., Petersen, S., Meyer, K., Casadío,
386   S., Speijer, R., and Claeys, P.: An assessment of latest Cretaceous Pycnodonte vesicularis (Lamarck,
387   1806) shells as records for palaeoseasonality: A multi-proxy investigation, Climate of the Past
388   Discussions, 2017, 1–36, 2017.

389   Deming, W. E.: Statistical adjustment of data., 1943.

390   Dennis, K. J. and Schrag, D. P.: Clumped isotope thermometry of carbonatites as an indicator of
391   diagenetic alteration, Geochimica et Cosmochimica Acta, 74, 4110–4122,
392   https://doi.org/10.1016/j.gca.2010.04.005, 2010.

393   Dennis, K. J., Affek, H. P., Passey, B. H., Schrag, D. P., and Eiler, J. M.: Defining an absolute reference
394   frame for 'clumped' isotope studies of CO2, Geochimica et Cosmochimica Acta, 75, 7117–7131,
395   https://doi.org/10.1016/j.gca.2011.09.025, 2011.

396   Dennis, K. J., Cochran, J. K., Landman, N. H., and Schrag, D. P.: The climate of the Late Cretaceous:
397   New insights from the application of the carbonate clumped isotope thermometer to Western
398   Interior Seaway macrofossil, Earth and Planetary Science Letters, 362, 51–65,
399   https://doi.org/10.1016/j.epsl.2012.11.036, 2013.

400   Dong, J., Eiler, J., An, Z., Li, X., Liu, W., and Hu, J.: Clumped isotopic compositions of cultured and
401   natural land-snail shells and their implications, Palaeogeography, Palaeoclimatology,
402   Palaeoecology, 577, 110530, https://doi.org/10.1016/j.palaeo.2021.110530, 2021.

403   Eiler, J. M.: "Clumped-isotope" geochemistry—The study of naturally-occurring, multiply-substituted
404   isotopologues, Earth and Planetary Science Letters, 262, 309–327,
405   https://doi.org/10.1016/j.epsl.2007.08.020, 2007.

406   EPSTEIN, S., BUCHSBAUM, R., LOWENSTAM, H. A., and UREY, H. C.: REVISED CARBONATE-WATER
407   ISOTOPIC TEMPERATURE SCALE, GSA Bulletin, 64, 1315–1326, https://doi.org/10.1130/0016-
408   7606(1953)64[1315:RCITS]2.0.CO;2, 1953.

409   Fernandez, A., Müller, I. A., Rodríguez-Sanz, L., van Dijk, J., Looser, N., and Bernasconi, S. M.: A
410   reassessment of the precision of carbonate clumped isotope measurements: implications for
411   calibrations and paleoclimate reconstructions, 18, 4375–4386, 2017.

412   Fiebig, J., Daëron, M., Bernecker, M., Guo, W., Schneider, G., Boch, R., Bernasconi, S. M., Jautzy, J.,
413   and Dietzel, M.: Calibration of the dual clumped isotope thermometer for carbonates, Geochimica
414   et Cosmochimica Acta, https://doi.org/10.1016/j.gca.2021.07.012, 2021.

415   Frisia, S., Borsato, A., Fairchild, I. J., and McDermott, F.: Calcite Fabrics, Growth Mechanisms, and
416   Environments of Formation in Speleothems from the Italian Alps and Southwestern Ireland,
417   Journal of Sedimentary Research, 70, 1183–1196, https://doi.org/10.1306/022900701183, 2000.

418   Ghosh, P., Adkins, J., Affek, H., Balta, B., Guo, W., Schauble, E. A., Schrag, D., and Eiler, J. M.: 13C–18O
419   bonds in carbonate minerals: A new kind of paleothermometer, Geochimica et Cosmochimica
420   Acta, 70, 1439–1456, https://doi.org/10.1016/j.gca.2005.11.014, 2006.

421   Ghosh, P., Eiler, J., Campana, S. E., and Feeney, R. F.: Calibration of the carbonate 'clumped isotope'
422   paleothermometer for otoliths, Geochimica et Cosmochimica Acta, 71, 2736–2744,
423   https://doi.org/10.1016/j.gca.2007.03.015, 2007.

424   Goodwin, D. H., Flessa, K. W., Schöne, B. R., and Dettman, D. L.: Cross-calibration of daily growth
425   increments, stable isotope variation, and temperature in the Gulf of California bivalve mollusk
426   Chione cortezi: implications for paleoenvironmental analysis, 16, 387–398, 2001.

Goodwin, D. H., Schöne, B. R., and Dettman, D. L.: Resolution and Fidelity of Oxygen Isotopes as Paleotemperature Proxies in Bivalve Mollusk Shells: Models and Observations, PALAIOS, 18, 110–125, https://doi.org/10.1669/0883-1351(2003)18<110:RAFOOI>2.0.CO;2, 2003.

Guo, W.: Kinetic clumped isotope fractionation in the DIC-H2O-CO2 system: Patterns, controls, and implications, Geochimica et Cosmochimica Acta, 268, 230–257, https://doi.org/10.1016/j.gca.2019.07.055, 2020.

Guo, W., Mosenfelder, J. L., Goddard, W. A., and Eiler, J. M.: Isotopic fractionations associated with phosphoric acid digestion of carbonate minerals: Insights from first-principles theoretical modeling and clumped isotope measurements, Geochimica et Cosmochimica Acta, 73, 7203–7225, https://doi.org/10.1016/j.gca.2009.05.071, 2009.

Hansen, H. J.: Test structure and evolution in the Foraminifera, 12, 173–182, https://doi.org/10.1111/let.1979.12.2.173, 1979.

He, B., Olack, G. A., and Colman, A. S.: Pressure baseline correction and high-precision CO2 clumped-isotope (Δ 47) measurements in bellows and micro-volume modes, 26, 2837–2853, 2012.

Henkes, G. A., Passey, B. H., Wanamaker, A. D., Grossman, E. L., Ambrose, W. G., and Carroll, M. L.: Carbonate clumped isotope compositions of modern marine mollusk and brachiopod shells, Geochimica et Cosmochimica Acta, 106, 307–325, https://doi.org/10.1016/j.gca.2012.12.020, 2013.

Henkes, G. A., Passey, B. H., Grossman, E. L., Shenton, B. J., Yancey, T. E., and Pérez-Huerta, A.: Temperature evolution and the oxygen isotope composition of Phanerozoic oceans from carbonate clumped isotope thermometry, Earth and Planetary Science Letters, 490, 40–50, https://doi.org/10.1016/j.epsl.2018.02.001, 2018.

Huyghe, D., Daëron, M., de Rafelis, M., Blamart, D., Sébilo, M., Paulet, Y.-M., and Lartaud, F.: Clumped isotopes in modern marine bivalves, Geochimica et Cosmochimica Acta, 316, 41–58, https://doi.org/10.1016/j.gca.2021.09.019, 2022.

Jautzy, J. J., Savard, M. M., Dhillon, R. S., Bernasconi, S. M., and Smirnoff, A.: Clumped isotope temperature calibration for calcite: Bridging theory and experimentation, 14, 36–41, 2020.

Kele, S., Breitenbach, S. F., Capezzuoli, E., Meckler, A. N., Ziegler, M., Millan, I. M., Kluge, T., Deák, J., Hanselmann, K., and John, C. M.: Temperature dependence of oxygen-and clumped isotope fractionation in carbonates: a study of travertines and tufas in the 6–95 C temperature range, 168, 172–192, 2015.

Kennedy, W. J., Taylor, J. D., and Hall, A.: Environmental and Biological Controls on Bivalve Shell Mineralogy, 44, 499–530, https://doi.org/10.1111/j.1469-185X.1969.tb00610.x, 1969.

Kim, S.-T. and O'Neil, J. R.: Equilibrium and nonequilibrium oxygen isotope effects in synthetic carbonates, Geochimica et Cosmochimica Acta, 61, 3461–3475, https://doi.org/10.1016/S0016-7037(97)00169-5, 1997.

Kimball, J., Eagle, R., and Dunbar, R.: Carbonate "clumped" isotope signatures in aragonitic scleractinian and calcitic gorgonian deep-sea corals, 13, 6487–6505, https://doi.org/10.5194/bg-13-6487-2016, 2016.

Kirchner, J.W. Data Analysis Toolkit #12: Weighted averages and their uncertaintie: http://seismo.berkeley.edu/~kirchner/Toolkits/Toolkit_12.pdf, last access: 3 August 2022.

Kluge, T., John, C. M., Jourdan, A.-L., Davis, S., and Crawshaw, J.: Laboratory calibration of the calcium carbonate clumped isotope thermometer in the 25–250°C temperature range, Geochimica et Cosmochimica Acta, 157, 213–227, https://doi.org/10.1016/j.gca.2015.02.028, 2015.

Knutti, R., Rugenstein, M. A. A., and Hegerl, G. C.: Beyond equilibrium climate sensitivity, Nature Geosci, 10, 727–736, https://doi.org/10.1038/ngeo3017, 2017.

473 Kocken, I. J., Müller, I. A., and Ziegler, M.: Optimizing the Use of Carbonate Standards to Minimize
474   Uncertainties in Clumped Isotope Data, 20, 5565–5577, https://doi.org/10.1029/2019GC008545,
475   2019.
476 Letulle, T., Suan, G., Daëron, M., Rogov, M., Lécuyer, C., Vinçon-Laugier, A., Reynard, B., Montagnac,
477   G., Lutikov, O., and Schlögl, J.: Clumped isotope evidence for Early Jurassic extreme polar warmth
478   and high climate sensitivity, 18, 435–448, https://doi.org/10.5194/cp-18-435-2022, 2022.
479 Masson-Delmotte, V., Zhai, P., Pirani, A., Connors, S. L., Péan, C., Berger, S., Caud, N., Chen, Y.,
480   Goldfarb, L., Gomis, M. I., Huang, M., Leitzell, K., Lonnoy, E., Matthews, J. B. R., Maycock, T. K.,
481   Waterfield, T., Yelekçi, Ö., Yu, R., and Zhou, B. (Eds.): Climate Change 2021: The Physical Science
482   Basis. Contribution of Working Group I to the Sixth Assessment Report of the Intergovernmental
483   Panel on Climate Change, Cambridge University Press, 2021.
484 Meckler, A. N., Ziegler, M., Millán, M. I., Breitenbach, S. F., and Bernasconi, S. M.: Long-term
485   performance of the Kiel carbonate device with a new correction scheme for clumped isotope
486   measurements, 28, 1705–1715, 2014.
487 Meinicke, N., Ho, S. L., Hannisdal, B., Nürnberg, D., Tripati, A., Schiebel, R., and Meckler, A. N.: A
488   robust calibration of the clumped isotopes to temperature relationship for foraminifers,
489   Geochimica et Cosmochimica Acta, 270, 160–183, https://doi.org/10.1016/j.gca.2019.11.022,
490   2020.
491 Meinicke, N., Reimi, M. A., Ravelo, A. C., and Meckler, A. N.: Coupled Mg/Ca and Clumped Isotope
492   Measurements Indicate Lack of Substantial Mixed Layer Cooling in the Western Pacific Warm Pool
493   During the Last ~5 Million Years, 36, e2020PA004115, https://doi.org/10.1029/2020PA004115,
494   2021.
495 Modestou, S. E., Leutert, T. J., Fernandez, A., Lear, C. H., and Meckler, A. N.: Warm Middle Miocene
496   Indian Ocean Bottom Water Temperatures: Comparison of Clumped Isotope and Mg/Ca-Based
497   Estimates, 35, e2020PA003927, https://doi.org/10.1029/2020PA003927, 2020.
498 Müller, I. A., Violay, M. E. S., Storck, J.-C., Fernandez, A., van Dijk, J., Madonna, C., and Bernasconi, S.
499   M.: Clumped isotope fractionation during phosphoric acid digestion of carbonates at 70°C,
500   Chemical Geology, 449, 1–14, https://doi.org/10.1016/j.chemgeo.2016.11.030, 2017.
501 Müller, I. A., Rodriguez-Blanco, J. D., Storck, J.-C., do Nascimento, G. S., Bontognali, T. R. R.,
502   Vasconcelos, C., Benning, L. G., and Bernasconi, S. M.: Calibration of the oxygen and clumped
503   isotope thermometers for (proto-)dolomite based on synthetic and natural carbonates, Chemical
504   Geology, 525, 1–17, https://doi.org/10.1016/j.chemgeo.2019.07.014, 2019.
505 Nooitgedacht, C. W., van der Lubbe, H. J. L., Ziegler, M., and Staudigel, P. T.: Internal Water Facilitates
506   Thermal Resetting of Clumped Isotopes in Biogenic Aragonite, 22, e2021GC009730,
507   https://doi.org/10.1029/2021GC009730, 2021.
508 Peral, M., Daëron, M., Blamart, D., Bassinot, F., Dewilde, F., Smialkowski, N., Isguder, G., Bonnin, J.,
509   Jorissen, F., and Kissel, C.: Updated calibration of the clumped isotope thermometer in planktonic
510   and benthic foraminifera, 239, 1–16, 2018.
511 Petersen, S. V., Tabor, C. R., Lohmann, K. C., Poulsen, C. J., Meyer, K. W., Carpenter, S. J., Erickson, J.
512   M., Matsunaga, K. K., Smith, S. Y., and Sheldon, N. D.: Temperature and salinity of the Late
513   Cretaceous western interior seaway, 44, 903–906, 2016.
514 Petersen, S. V., Defliese, W. F., Saenger, C., Daëron, M., Huntington, K. W., John, C. M., Kelson, J. R.,
515   Bernasconi, S. M., Colman, A. S., Kluge, T., Olack, G. A., Schauer, A. J., Bajnai, D., Bonifacie, M.,
516   Breitenbach, S. F. M., Fiebig, J., Fernandez, A. B., Henkes, G. A., Hodell, D., Katz, A., Kele, S.,
517   Lohmann, K. C., Passey, B. H., Peral, M. Y., Petrizzo, D. A., Rosenheim, B. E., Tripati, A., Venturelli,
518   R., Young, E. D., and Winkelstern, I. Z.: Effects of Improved 17O Correction on Interlaboratory
519   Agreement in Clumped Isotope Calibrations, Estimates of Mineral-Specific Offsets, and

520   Temperature Dependence of Acid Digestion Fractionation, 20, 3495–3519,
521   https://doi.org/10.1029/2018GC008127, 2019.

522 Piasecki, A., Bernasconi, S. M., Grauel, A.-L., Hannisdal, B., Ho, S. L., Leutert, T. J., Marchitto, T. M.,
523   Meinicke, N., Tisserand, A., and Meckler, N.: Application of Clumped Isotope Thermometry to
524   Benthic Foraminifera, 20, 2082–2090, https://doi.org/10.1029/2018GC007961, 2019.

525 R Core Team: R: A Language and Environment for Statistical Computing, R Foundation for Statistical
526   Computing, Vienna, Austria, 2022.

527 Rodríguez-Sanz, L., Bernasconi, S. M., Marino, G., Heslop, D., Müller, I. A., Fernandez, A., Grant, K. M.,
528   and Rohling, E. J.: Penultimate deglacial warming across the Mediterranean Sea revealed by
529   clumped isotopes in foraminifera, Sci Rep, 7, 16572, https://doi.org/10.1038/s41598-017-16528-
530   6, 2017.

531 Schaefer, R., Trutschler, K., and Rumohr, H.: Biometric studies on the bivalvesAstarte elliptica, A.
532   borealis andA. montagui in Kiel Bay (Western Baltic Sea), Helgolander Meeresunters, 39, 245–253,
533   https://doi.org/10.1007/BF01992772, 1985.

534 Schauble, E. A., Eiler, J. M., and Kitchen, N.: Measurement and significance of ^(13)C^(18)O^(16)O in
535   thermodynamically equilibrated and environmental CO_2, 67, A419–A419, 2003.

536 Schauble, E. A., Ghosh, P., and Eiler, J. M.: Preferential formation of 13C–18O bonds in carbonate
537   minerals, estimated using first-principles lattice dynamics, Geochimica et Cosmochimica Acta, 70,
538   2510–2529, https://doi.org/10.1016/j.gca.2006.02.011, 2006.

539 Schöne, B. R. and Fiebig, J.: Seasonality in the North Sea during the Allerød and Late Medieval
540   Climate Optimum using bivalve sclerochronology, 98, 83–98, 2009.

541 Schöne, B. R., Fiebig, J., Pfeiffer, M., Gleβ, R., Hickson, J., Johnson, A. L., Dreyer, W., and Oschmann,
542   W.: Climate records from a bivalved Methuselah (Arctica islandica, Mollusca; Iceland), 228, 130–
543   148, 2005.

544 Staudigel, P. T. and Swart, P. K.: Isotopic behavior during the aragonite-calcite transition: Implications
545   for sample preparation and proxy interpretation, Chemical Geology, 442, 130–138,
546   https://doi.org/10.1016/j.chemgeo.2016.09.013, 2016.

547 Sturm, P.: bfsl: Best-Fit Straight Line, 2018.

548 Swart, P. K., Lu, C., Moore, E. W., Smith, M. E., Murray, S. T., and Staudigel, P. T.: A calibration
549   equation between Δ48 values of carbonate and temperature, 35, e9147,
550   https://doi.org/10.1002/rcm.9147, 2021.

551 Tatebe, K. Combining Multiple Averaged Data Points And Their Errors:
552   https://docplayer.net/33088897-Combining-multiple-averaged-data-points-and-their-errors.html,
553   last access: 3 August 2022.

554 Taylor, J. D. and Reid, D. G.: Shell microstructure and mineralogy of the Littorinidae: ecological and
555   evolutionary significance, in: Progress in Littorinid and Muricid Biology, Dordrecht, 199–215,
556   https://doi.org/10.1007/978-94-009-0563-4_16, 1990.

557 Tierney, J. E., Poulsen, C. J., Montañez, I. P., Bhattacharya, T., Feng, R., Ford, H. L., Hönisch, B., Inglis,
558   G. N., Petersen, S. V., Sagoo, N., Tabor, C. R., Thirumalai, K., Zhu, J., Burls, N. J., Foster, G. L.,
559   Goddéris, Y., Huber, B. T., Ivany, L. C., Turner, S. K., Lunt, D. J., McElwain, J. C., Mills, B. J. W., Otto-
560   Bliesner, B. L., Ridgwell, A., and Zhang, Y. G.: Past climates inform our future, 370,
561   https://doi.org/10.1126/science.aay3701, 2020.

562 Tripati, A. K., Eagle, R. A., Thiagarajan, N., Gagnon, A. C., Bauch, H., Halloran, P. R., and Eiler, J. M.:
563   13C–18O isotope signatures and 'clumped isotope' thermometry in foraminifera and coccoliths,
564   Geochimica et Cosmochimica Acta, 74, 5697–5717, https://doi.org/10.1016/j.gca.2010.07.006,
565   2010.

566 Urey, H. C.: The thermodynamic properties of isotopic substances - Google Scholar, 562–581, 1947.

567 Vickers, M. L., Lengger, S. K., Bernasconi, S. M., Thibault, N., Schultz, B. P., Fernandez, A., Ullmann, C.
568   V., McCormack, P., Bjerrum, C. J., Rasmussen, J. A., Hougård, I. W., and Korte, C.: Cold spells in the
569   Nordic Seas during the early Eocene Greenhouse, Nat Commun, 11, 4713,
570   https://doi.org/10.1038/s41467-020-18558-7, 2020a.

571 Vickers, M. L., Fernandez, A., Hesselbo, S. P., Price, G. D., Bernasconi, S. M., Lode, S., Ullmann, C. V.,
572   Thibault, N., Hougaard, I. W., and Korte, C.: Unravelling Middle to Late Jurassic
573   palaeoceanographic and palaeoclimatic signals in the Hebrides Basin using belemnite clumped
574   isotope thermometry, Earth and Planetary Science Letters, 546, 116401,
575   https://doi.org/10.1016/j.epsl.2020.116401, 2020b.

576 Wacker, U., Fiebig, J., and Schoene, B. R.: Clumped isotope analysis of carbonates: comparison of two
577   different acid digestion techniques, 27, 1631–1642, 2013.

578 Wacker, U., Fiebig, J., Tödter, J., Schöne, B. R., Bahr, A., Friedrich, O., Tütken, T., Gischler, E., and
579   Joachimski, M. M.: Empirical calibration of the clumped isotope paleothermometer using calcites
580   of various origins, 141, 127–144, 2014.

581 Wang, Z., Schauble, E. A., and Eiler, J. M.: Equilibrium thermodynamics of multiply substituted
582   isotopologues of molecular gases, Geochimica et Cosmochimica Acta, 68, 4779–4797,
583   https://doi.org/10.1016/j.gca.2004.05.039, 2004.

584 Westerhold, T., Marwan, N., Drury, A. J., Liebrand, D., Agnini, C., Anagnostou, E., Barnet, J. S., Bohaty,
585   S. M., De Vleeschouwer, D., and Florindo, F.: An astronomically dated record of Earth's climate
586   and its predictability over the last 66 million years, 369, 1383–1387, 2020.

587 de Winter, N. J., Vellekoop, J., Clark, A. J., Stassen, P., Speijer, R. P., and Claeys, P.: The giant marine
588   gastropod Campanile giganteum (Lamarck, 1804) as a high-resolution archive of seasonality in the
589   Eocene greenhouse world, 21, e2019GC008794, https://doi.org/10.1029/2019GC008794, 2020.

590 de Winter, N. J., Müller, I. A., Kocken, I. J., Thibault, N., Ullmann, C. V., Farnsworth, A., Lunt, D. J.,
591   Claeys, P., and Ziegler, M.: Absolute seasonal temperature estimates from clumped isotopes in
592   bivalve shells suggest warm and variable greenhouse climate, Commun Earth Environ, 2, 1–8,
593   https://doi.org/10.1038/s43247-021-00193-9, 2021a.

594 de Winter, N. J., Dämmer, L. K., Falkenroth, M., Reichart, G.-J., Moretti, S., Martínez-García, A.,
595   Höche, N., Schöne, B. R., Rodiouchkina, K., Goderis, S., Vanhaecke, F., van Leeuwen, S. M., and
596   Ziegler, M.: Multi-isotopic and trace element evidence against different formation pathways for
597   oyster microstructures, Geochimica et Cosmochimica Acta, 308, 326–352,
598   https://doi.org/10.1016/j.gca.2021.06.012, 2021b.

599 de Winter, Niels J., Witbaard, Rob, Kocken, Ilja J., Müller, Inigo A., Guo, Jingjing, Goudsmit, Barbara, &
600   Ziegler, Martin. (2022). Supplementary Information for "Temperature dependence of clumped
601   isotopes (Δ47) in aragonite". https://doi.org/10.5281/zenodo.6524706

602 de Winter, N. J.: R Scripts belowing to: Temperature dependence of clumped isotopes (Δ47) in
603   aragonite, GitHub, https://github.com/nielsjdewinter/Aragonite_clumped, 2022.Witbaard, R.,
604   Duineveld, G. C. A., and De Wilde, P.: A long-term growth record derived from Arctica islandica
605   (Mollusca, Bivalvia) from the Fladen Ground (northern North Sea), 77, 801–816, 1997.

606 Witbaard, R., Franken, R., and Visser, B.: Growth of juvenileArctica islandica under experimental
607   conditions, Helgoländer Meeresunters., 51, 417, https://doi.org/10.1007/BF02908724, 1998.

608 Zhai, J., Wang, X., Qin, B., Cui, L., Zhang, S., and Ding, Z.: Clumped isotopes in land snail shells over
609   China: Towards establishing a biogenic carbonate paleothermometer, Geochimica et
610   Cosmochimica Acta, 257, 68–79, https://doi.org/10.1016/j.gca.2019.04.028, 2019.

611 Zhang, N., Yamada, K., Kano, A., Matsumoto, R., and Yoshida, N.: Equilibrated clumped isotope
612   signatures of land-snail shells observed from laboratory culturing experiments and its
613   environmental implications, Chemical Geology, 488, 189–199,
614   https://doi.org/10.1016/j.chemgeo.2018.05.001, 2018.

Table 1 *Arctica islandica* clumped isotope results compared to previous calibrations

"mixed" = combined samples from multiple specimens, number codes (e.g. "29" or "6A") = material from one individual. "Ais" = *Arctica islandica*. Significant Δ_{47} and temperature offsets are labeled in bold. cc = calcite, ar = aragonite

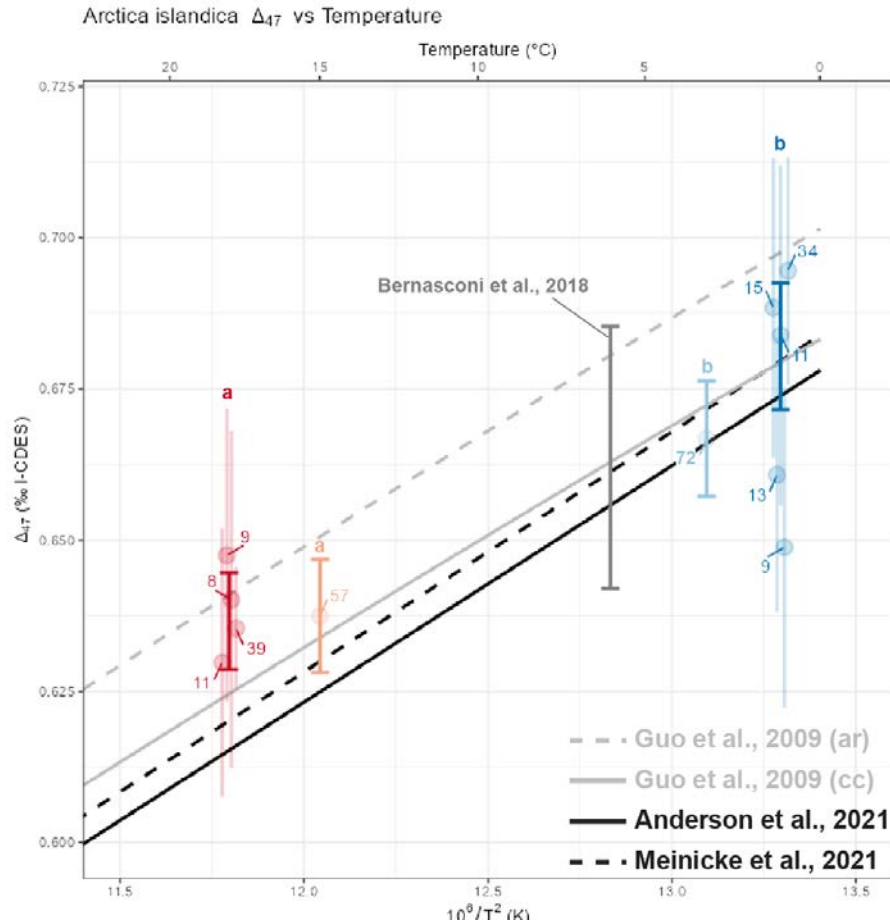| Sample	Culturing temperature	Δ_{47} (I-CDES; ± 95%CL)		N	Offset from Anderson	Offset from Meinicke	Offset from Guo (cc)	Offset from Guo (ar)
Ais1	1.1 ± 0.2°C	mixed	0.695 ± 0.019‰	34				
		3	0.661 ± 0.023‰	13				
		29	0.688 ± 0.025‰	15				
		6A	0.684 ± 0.028‰	11				
		6B	0.649 ± 0.026‰	9				
		TOTAL	0.682 ± 0.010‰	82	+0.008‰ -2.12°C	+0.002‰ -0.61°C	+0.003‰ -0.75°C	**−0.016‰ +4.48°C**
Ais3	3.2 ± 0.3°C	mixed	0.667 ± 0.010‰	72	+0.001‰ -0.27°C	−0.005‰ +1.24°C	−0.006‰ +1.57°C	**−0.023‰ +6.80°C**
Ais15	15 ± 0.4°C	mixed	0.637 ± 0.009‰	57	**+0.013‰ -3.63°C**	+0.008‰ -2.10°C	+0.004‰ -0.99°C	**−0.013‰ +4.25°C**
Ais18	18 ± 0.3°C	mixed	0.635 ± 0.010‰	39				
		67	0.647 ± 0.024‰	9				
		89	0.640 ± 0.028‰	8				
		111	0.630 ± 0.022‰	11				
		TOTAL	0.637 ± 0.005‰	67	**+0.021‰ -6.63°C**	**+0.016‰ -5.10°C**	**+0.012‰ -3.99°C**	−0.004‰ +1.25°C

Figure 1: *Arctica islandica* Δ_{47} results. Clumped isotope results are aggregated by specimen or multi-specimen sample (round symbols; see **Table 1**). Vertical lines represent 95% CL and number indicate sample size. Data is color-coded per temperature treatment (1°C, 3°C, 15°C and 18°C), with bold error bars indicating 95% CL, pairs of letter labels (a and b) indicate statistically indistinguishable Δ_{47} values ($p < 0.05$). The grey error bar at 6°C highlights *A. islandica* data from Bernasconi et al. (2018; recalculated to I-CDES). Solid and dashed black lines show calibrations by Anderson et al. (2021) and Meinicke et al. (2020; projected on I-CDES scale; Meinicke et al., 2021), respectively. Grey solid and dashed lines represent, respectively, the theoretical calcite ("cc") and aragonite ("ar") temperature dependencies from Guo et al. (2009; projected on the I-CDES scale, see **S1**). The horizontal axis is scaled to $\frac{10^6}{T^2}$, with T in K, to show the assumed linear relationship with the clumped isotope value.
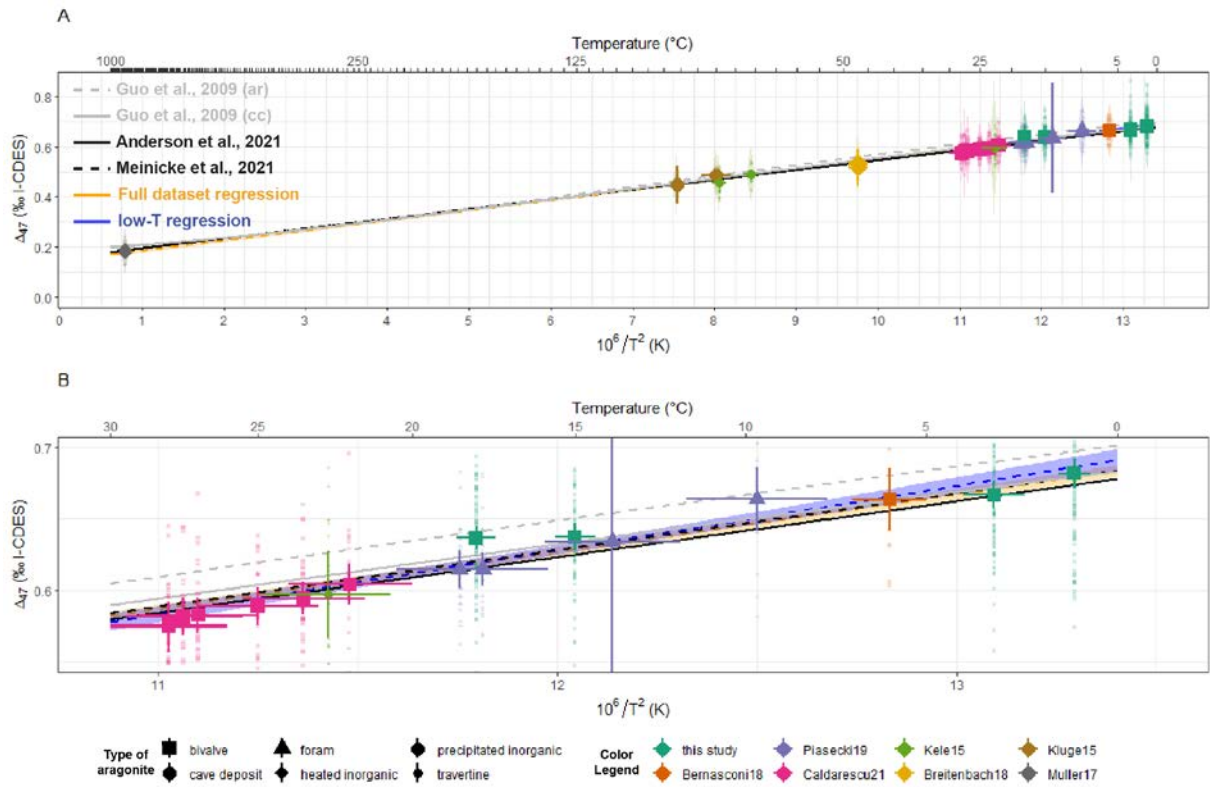
Figure 2: Aragonite Δ_{47} temperature dependence. Clumped isotope data of aragonite samples plotted against formation temperature. **A**. All data plotted over the full temperature range (1°C–850°C). Individual datapoints, averages and uncertainty on temperature and Δ_{47} values (95% CL) are color-coded by study. Symbols highlight different types of aragonite. The solid and dashed black lines show calibrations by Anderson et al. (2021) and Meinicke et al. (2020; 2021; plotted for temperatures <30°C). Grey solid and dashed lines represent, respectively, the theoretical calcite ("cc") and aragonite ("ar") temperature dependencies from Guo et al. (2009; projected on the I-CDES scale, see **section 2.5**). Colored dashed lines and shaded envelopes show York regressions through aragonite data and their 95% confidence envelopes, respectively. **B**. Shows a zoom-in of the plot in **A**. for the low-temperature domain (1–30°C). Note that the horizontal axis is scaled to $\frac{10^6}{T^2}$, with T in K, to show the assumed linear relationship with the clumped isotope value.
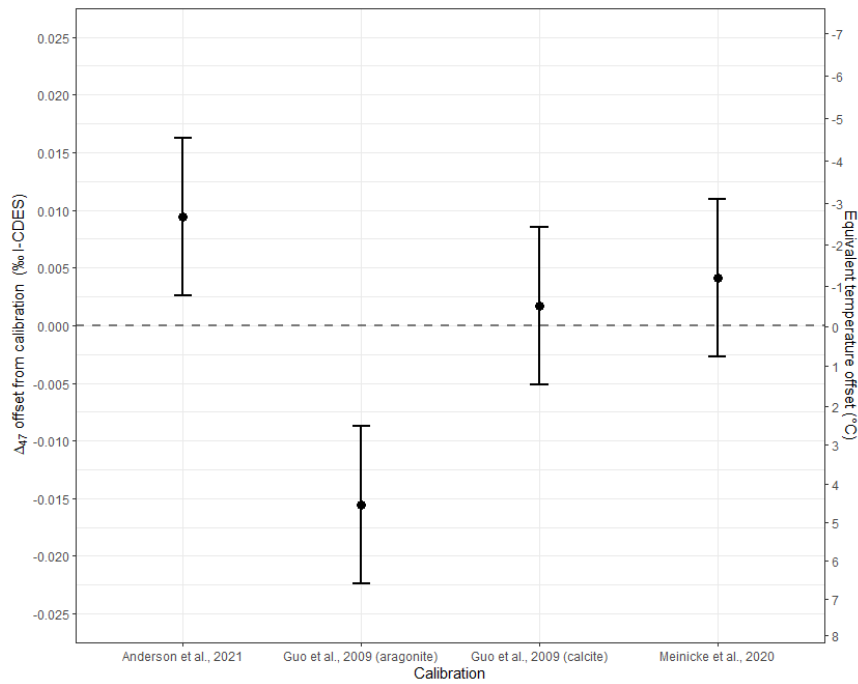
Figure 3: **Offset of *A. islandica* data from temperature regressions**. Shaded grey points show residual Δ_{47} values relative to four clumped isotope temperature relationships (see horizontal axis). Black symbols with error bars (95% CL) show mean offsets of all *A. islandica* datapoints (grown at 1°C, 3°C, 6°C, 15°C and 18°C) from the calibrations. The vertical axis on the right shows the temperature offset relative to the weighted mean calcification temperature of the full *A. islandica* dataset (8.6°C; see **S4**) based on Anderson et al. (2021).

Temperature dependence of clumped isotopes (Δ_{47}) in aragonite

Niels J. de Winter[1,2], Rob Witbaard[3], Ilja J. Kocken[2], Inigo A. Müller[4], Jingjing Guo[2], Barbara Goudsmit[2,3], Martin Ziegler[2]

1Analytical, Environmental and Geochemistry Group, Vrije Universiteit Brussel, Belgium

2Dept. of Earth Sciences, Utrecht University, the Netherlands

3Dept. of Estuarine and Delta Systems, Royal Netherlands Institute for Sea Research, the Netherlands.

4Isotope Geochemistry, Geochronology and Thermochronology group, Earth and Environmental Science, Université de Genève, Switzerland

Contents of this file

Introduction

This Supplement contains all supplementary text and figures for the manuscript. All data files, scripts and large tables are deposited in the accompanying Zenodo repository (https://doi.org/10.5281/zenodo.6524705, see Open Research chapter).

Text S1: Supplementary Methodology

1. Culture experiments

Living specimens of juvenile *Arctica islandica* (bivalvia) were collected from the Süderfart site in

the Kieler Bucht to the north-east of Kiel, Germany (54°34'11"N, 10°51'59"E; see Schaefer et al.,

1985). All animals were placed in sand-filled containers in a basin with aerated seawater which

was refreshed two days a week with water from the Marsdiep tidal inlet directly outside the Royal Netherlands Institute for Sea Research (NIOZ, Texel, the Netherlands; 53°00'04"N, 4°47'23"E). Specimens used for this study were grown under four different, constant, and monitored temperature regimes: 1.1 ± 0.2°C, 3.2 ± 0.3°C, 15 ± 0.4°C and 18 ± 0.3°C and fed *ad libidum* with a suspension of *Isochrysis galbana* and *Dunaliella marina* algae. Specimens were left to acclimatize to the culturing conditions for four weeks. During the experiments, shell growth, temperature, phytoplankton cell counts, chlorophyll concentration, particulate organic carbon content and siphon activity were monitored. The experiment lasted for 95 days, after which the specimens were euthanized, and soft tissue was removed from the shells. Clean shells were rinsed with fresh water, dried at room temperature (~20°C), and stored under cool and dry conditions after the growth experiment. Additional details on the growing conditions of the specimens and the setup of the experiments can be found in Witbaard et al. (1998).

2. Sampling strategy

Aragonite from cleaned and dried shells from these lab-grown *Arctica islandica* specimens was sampled using a hand-held Dremel 3000 rotary drill at low speed equipped with a tungsten-carbide drill bit. Minimal pressure was applied to carefully flake off parts of the shell and prevent heating of the samples due to friction, which may alter the Δ_{47} value of the aragonite (Staudigel and Swart, 2016). Care was taken to only sample the part of the shells that grew during the experiment. Pre-experimental shell material was easily avoided due to a clear growth line and color change that separated natural from lab-grown shell material (see **Fig. S1**).

3. Clumped isotope analyses

Aragonite aliquots were reacted with nominally anhydrous (103%) phosphoric acid at 70°C. The produced CO_2 gas was led through two liquid nitrogen-cooled (−196°C) cryogenic traps and a

2

PoraPak™ Q trap (Merck KGaA, Darmstadt, Germany) kept at −40°C or (after October 2020) −50°C through a custom-built external cooling unit (Dennis and Schrag, 2010). The purified CO_2 gas was analyzed in micro-volume mode using the LIDI workflow with 400 s integration time against a clean CO_2 working gas ($\delta^{13}C$ = −2.82‰; $\delta^{18}O$ = −4.67‰) and corrected for pressure baseline effects (Bernasconi et al., 2013; Meckler et al., 2014; Müller et al., 2017). Clumped isotope values were corrected to the Intercarb-Carbon Dioxide Equilibrium Scale (I-CDES) by creating an empirical transfer function (ETF) using measurements of ETH standards (ETH-1, -2 and -3) and their accepted Intercarb values (Bernasconi et al., 2021). We applied the ETF in a moving window of 200 analyses before and after the sample, considering standards measured within a time window of 2–3 weeks surrounding the sample for its correction. This typically resulted in 13 ETH-1, 13 ETH-2 and 70 ETH-3 measurements to constrain the ETF for each sample aliquot. Higher amounts of ETH-3 standards were analyzed to better constrain uncertainties around the expected Δ_{47} values of samples (Kocken et al., 2019). Measurements of the ETH-3 standard were also included every 3–5 samples to check for measurement drift at shorter timescales than the moving window of the ETF.

4. Data compilation

All included datasets except for Kluge et al. (2015) reported measured values for the ETH-1, -2 and -3 standards, yielding three anchor points for the reference scale calibration. The Kluge et al. (2015) data was calibrated to I-CDES using the ETH-3 and Carrara marble standard using the simplified linear correction in Appendix A of Bernasconi et al. (2021). To obtain an I-CDES Δ_{47} value for the Carrara marble standard (which is not reported in Bernasconi et al., 2021), we averaged the 19 replicates of Carrara marble reported in Bernasconi et al. (2018) after correcting their values to the I-CDES scale through the ETH standards, resulting in a value of 0.325 ± 0.008‰ (95% confidence level).

Where possible, we used means and standard deviations of the calcification temperature of the samples as reported in the literature. Measurement uncertainty was often reported at the level of standard errors on the mean of multiple aliquots of the same sample. The standard deviation of Δ_{47} values on individual aliquots was estimated from repeated measurements of reference materials not involved in the calibration (e.g. ETH-4 or Carrara marble) or, if these were not reported, by back-calculating the standard deviation from the standard error through multiplication by the square root of the sample size. In absence of uncertainties on the calcification temperature, the standard deviation of the temperatures was assumed to be 1°C for samples in the low-temperature domain (<100°C) and 10°C for high-temperature samples (the 850°C heated aragonites from Müller et al., 2017).

The Guo et al. (2009) temperature dependencies were brought into the I-CDES reference frame by updating the Δ_{47}-Δ_{63} fractionation factor to 0.268‰ (following Dennis et al., 2011), applying the Δ_{47}-dependent scaling of the Δ_{47}-Δ_{63} fractionation factor of 35 ppm/‰ (cited in Guo et al., 2009 and implemented in Jautzy et al., 2020) and calibrating to the I-CDES scale using a linear calibration through the Δ_{47} values of ETH-1 and ETH-3. For this calibration, the "new" I-CDES values for ETH-1 and ETH-3 were retrieved from Bernasconi et al. (2021) and the "old" CDES25 (CDES with reference to a reaction temperature of 25°C) values were obtained by solving the polynomial functions for the formation temperatures of the ETH standards (assumed to be 20°C for ETH-3 and 600°C for ETH-1, following Meckler et al., 2014).

5. Statistical evaluation

Differences between temperatures and between specimens within the same temperature treatment were tested using a one-way ANOVA and post-hoc Tukey multiple pairwise comparisons (see **S5**). Uncertainties on Δ_{47} values and calcification temperatures on the aliquot level are propagated through all statistical procedures, and uncertainty-weighted means and 95% confidence levels of samples are used for plotting throughout the manuscript (see section 6 below). The difference in

reproducibility between aliquots measured on our MAT253 (σ of reproducibility of IAEA-C2 of 0.046‰) and our MAT253 plus (σ of reproducibility of IAEA-C2 of 0.026‰) was considered in our error propagation by initially grouping aliquots by instrument and summarizing statistics (means and σ). The weighted mean and uncertainty of all aliquots from the same specimen or treatment group, but measured on different instruments, was then calculated by combining the statistics of groups of aliquots from the two machines and weighting the contribution of the two instrument groups by the factor $\frac{N}{\sigma^2}$, in which N is the number of aliquots in the instrument group and σ is the standard deviation representing the reproducibility within the group. For the value of σ, either the external standard deviation based on IAEA-C2 measurements on that instrument was used or the standard deviation between the Δ_{47} values of the aliquots within the group, whichever yielded the largest (and therefore most conservative) estimate of the uncertainty. This approach was based on work by Tatebe (2005) and Kirchner (2006) and the calculations are worked out in detail below (derivation) and **S5** (R script). To incorporate uncertainty on both Δ_{47} values and calcification temperatures at the aliquot level into our regressions, we apply a York regression (York, 1966) that takes into account errors on the independent variable as implemented in the "bfsl" R package by Patrick Sturm (Sturm, 2018). This linear York regression is repeated for the full dataset and for the dataset excluding high temperature (>30°C) datapoints to test the effect of these measurements on the regression. Throughout these statistical evaluations, it is assumed that uncertainties on Δ_{47} values and calcification temperatures are normally distributed.

6. Calculating weighted means and standard deviations

Suppose we have a dataset of measurements that measure the same quantity with different uncertainty. This difference in uncertainty can be taken into account when determining the mean and standard deviation of the dataset. In this document we derive equations for the weighted mean and standard deviation for a dataset of raw measurements, and for a dataset consisting pre-binned data in two or more bins.

6.1 Dataset of individual measurements

Suppose we have a dataset consisting of several raw measurements, all with their own uncertainty. The mean and standard deviation of the dataset can be calculated by weighting the measurements, and the optimal choice of weights is based on the inverse of the measurement variance (Kirchner, 2006).

To put this in mathematical terms: we have a dataset of n measurements $x_1, \ldots, x_n$ each with known variance $\sigma_1^2, \ldots, \sigma_n^2$ (note that we express the variance as the square of the standard deviation σ). In order to calculate the weighted mean μ and standard deviation σ, we define weights $w_i = 1/\sigma_i^2 = \sigma_i^{-2}$ for $i = 1, \ldots, n$. Following equations (1) and (2) of Kirchner, (2006), we find:

$$\mu = \frac{\sum_{i=1}^{n} w_i \cdot x_i}{\sum_{i=1}^{n} w_i}$$

(1)

$$\sigma = \sqrt{\frac{n}{n-1} \cdot \frac{\sum_{i=1}^{n} w_i \cdot (x_i - \mu)^2}{\sum_{i=1}^{n} w_i}}$$

(2)

Note that in case of equal weights for all measurements (i.e. $w_i = 1$ for $i = 1, \ldots, n$), Equations (1) and (2) coincide with the well-known formulas for unweighted mean and standard deviation:

$$\mu = \frac{\sum_{i=1}^{n} 1 \cdot x_i}{\sum_{i=1}^{n} 1} = \frac{\sum_{i=1}^{n} x_i}{n}$$

$$\sigma = \sqrt{\frac{n}{n-1} \cdot \frac{\sum_{i=1}^{n} 1 \cdot (x_i - \mu)^2}{\sum_{i=1}^{n} 1}} = \sqrt{\frac{n}{n-1} \cdot \frac{\sum_{i=1}^{n} (x_i - \mu)^2}{n}} = \sqrt{\frac{\sum_{i=1}^{n} (x_i - \mu)^2}{n-1}}$$

6.2 Binned datasets

Consider now the situation where the raw measurements have been binned in two or more bins. We know the mean, standard deviation, and bin size of the bins. From this information, we can estimate the weighted mean and standard deviation of the combination of bins. In this case, we weight the measurements using the inverse of the bin variance.

6.3 Dataset of two bins

First suppose we have two bins. Let's put this in mathematical terms again. We have two bins: B_1 with mean μ_1, standard deviation σ_1, and size n_1, and B_2 with mean μ_2, standard deviation σ_2, and size n_2. Bin B_1 consists of (unknown) measurements $y_1, \ldots, y_{n_1}$, and B_2 consists of (unknown) measurements $z_1, \ldots, z_{n_2}$. The combination of the bins has size $n = n_1 + n_2$ and consists of (unknown) measurements $x_1, \ldots, x_n = y_1, \ldots, y_{n_1}, z_1, \ldots, z_{n_2}$. We want to estimate the weighted mean and standard deviation using weights $w_1 = 1/\sigma_1^2$ for the measurements of B_1, and $w_2 = 1/\sigma_2^2$ for the measurements of B_2. The derivations in this section were inspired by the analysis of Tatebe (2005).

For the weighted mean, we apply Equation (1) to find:

$$\mu \quad = \frac{\sum_{i=1}^{n} w_i \cdot x_i}{\sum_{i=1}^{n} w_i} \qquad \text{Apply Equation (1)}$$

$$= \frac{\sum_{i=1}^{n_1} w_1 \cdot y_i + \sum_{i=1}^{n_2} w_2 \cdot z_i}{\sum_{i=1}^{n_1} w_1 + \sum_{i=1}^{n_2} w_2} \qquad \text{Split sums into the two bins}$$

$$= \frac{w_1 \cdot \sum_{i=1}^{n_1} y_i + w_2 \cdot \sum_{i=1}^{n_2} z_i}{n_1 \cdot w_1 + n_2 \cdot w_2} \qquad \text{The weights in the sums are constants, so the sums can be simplified}$$

$$= \frac{w_1 \cdot n_1 \cdot \mu_1 + w_2 \cdot n_2 \cdot \mu_2}{n_1 \cdot w_1 + n_2 \cdot w_2} \qquad \text{For } B_1 \text{ we have } \sum_{i=1}^{n_1} y_i = n_1 \cdot \mu_1, \qquad (3)$$

7

and a similar relation holds for B_2.

Note that in case of equal weighting (i.e., $w_1 = w_2 = 1$), Equation (3) comes down to a weighted mean that only takes the difference in bin size into account.

The derivation for the weighted standard deviation is more elaborate. First, we apply Equation (2). Using the same line of reasoning as for the mean, we find:

$$\sigma \quad = \sqrt{\frac{n}{n-1} \cdot \frac{\sum_{i=1}^{n} w_i \cdot (x_i - \mu)^2}{\sum_{i=1}^{n} w_i}}$$

$$= \sqrt{\frac{n}{n-1} \cdot \frac{\sum_{i=1}^{n_1} w_1 \cdot (y_i - \mu)^2 + \sum_{i=1}^{n_2} w_2 \cdot (z_i - \mu)^2}{\sum_{i=1}^{n_1} w_1 + \sum_{i=1}^{n_2} w_2}}$$

$$= \sqrt{\frac{n}{n-1} \cdot \frac{w_1 \cdot \sum_{i=1}^{n_1} (y_i - \mu)^2 + w_2 \cdot \sum_{i=1}^{n_2} (z_i - \mu)^2}{n_1 \cdot w_1 + n_2 \cdot w_2}} \tag{4}$$

We can rewrite the terms $\sum_{i=1}^{n_1} (y_i - \mu)^2$ and $\sum_{i=1}^{n_2} (z_i - \mu)^2$ to eliminate the unknown measurements y_i and z_i from the equation. We consider the first term and note that the same line of reasoning holds for the second term. The keys to rewriting the terms are first adding $(\mu_1 - \mu_1) = 0$ to the sum, and then writing out the product of sums in separate sums:

$$\sum_{i=1}^{n_1} (y_i - \mu)^2 \quad = \sum_{i=1}^{n_1} \left((y_i - \mu_1) + (\mu_1 - \mu) \right)^2$$

$$= \sum_{i=1}^{n_1} (y_i - \mu_1)^2 + 2\,(y_i - \mu_1) \cdot (\mu_1 - \mu) + (\mu_1 - \mu)^2$$

$$= \sum_{i=1}^{n_1} (y_i - \mu_1)^2 + \sum_{i=1}^{n_1} 2\,(y_i - \mu_1) \cdot (\mu_1 - \mu) + \sum_{i=1}^{n_1} (\mu_1 - \mu)^2 \tag{5}$$

We rewrite each of the three sums in Equation (5) separately. For the first sum, we use the formula of the (unweighted) standard deviation applied to bin B_1:

$$\sum_{i=1}^{n_1} (y_i - \mu_1)^2 \qquad = (n_1 - 1) \cdot \sigma_1^2 \tag{6}$$

For the second sum, we note that $(\mu_1 - \mu)$ is a constant, so we can take it out of the summation:

$$
\begin{aligned}
\sum_{i=1}^{n_1} 2\,(y_i - \mu_1) \cdot (\mu_1 - \mu) \qquad &= 2 \cdot (\mu_1 - \mu) \cdot \sum_{i=1}^{n_1}(y_i - \mu_1) \\
&= 2 \cdot (\mu_1 - \mu) \cdot \left(\sum_{i=1}^{n_1} y_i - \sum_{i=1}^{n_1} \mu_1 \right) \\
&= 2 \cdot (\mu_1 - \mu) \cdot \left(n_1 \cdot \mu_1 - \sum_{i=1}^{n_1} \mu_1 \right) \\
&= 2 \cdot (\mu_1 - \mu) \cdot (n_1 \cdot \mu_1 - n_1 \cdot \mu_1) \\
&= 0
\end{aligned}
\tag{7}
$$

For the third sum, we again use that $(\mu_1 - \mu)$ is a constant:

$$\sum_{i=1}^{n_1} (\mu_1 - \mu)^2 \qquad = n_1 \cdot (\mu_1 - \mu)^2 \tag{8}$$

Plugging Equations (6), (7) and (8) in Equation (5), we find:

$$
\begin{aligned}
\sum_{i=1}^{n_1} (y_i - \mu)^2 \qquad &= \sum_{i=1}^{n_1}(y_i - \mu_1)^2 + \sum_{i=1}^{n_1} 2\,(y_i - \mu_1) \cdot (\mu_1 - \mu) + \sum_{i=1}^{n_1}(\mu_1 - \mu)^2 \\
&= (n_1 - 1) \cdot \sigma_1^2 + n_1 \cdot (\mu_1 - \mu)^2
\end{aligned}
\tag{9}
$$

The same derivation yields:

$$\sum_{i=1}^{n_2} (z_i - \mu)^2 \qquad = (n_2 - 1) \cdot \sigma_2^2 + n_2 \cdot (\mu_2 - \mu)^2 \tag{10}$$

Plugging Equations (9) and (10) in Equation (4), the formula for the weighted standard deviation becomes:

$$\sigma \quad = \sqrt{\frac{n}{n-1} \cdot \frac{w_1 \cdot (n_1-1) \cdot \sigma_1^2 + w_1 \cdot n_1 \cdot (\mu_1 - \mu)^2 + w_2 \cdot (n_2-1) \cdot \sigma_2^2 + w_2 \cdot n_2 \cdot (\mu_2 - \mu)^2}{n_1 \cdot w_1 + n_2 \cdot w_2}} \tag{11}$$

This equation consists of all known values, making use of Equation (3) for the mean μ. Note that in case of equal weighting (i.e., $w_1 = w_2 = 1$), Equation (11) comes down to an unweighted

9

standard deviation of all measurements in the two bins in relation to the mean of Equation (3).

Equation (11) can also be written in terms of only the characteristics of the two bins, by plugging Equation (3) in Equation (11) and rewriting the outcome. Consider the term $(\mu_1 - \mu)^2$. We can write:

$$(\mu_1 - \mu)^2 \qquad = \left(\mu_1 - \frac{w_1 \cdot n_1 \cdot \mu_1 + w_2 \cdot n_2 \cdot \mu_2}{n_1 \cdot w_1 + n_2 \cdot w_2}\right)^2$$

$$= \left(\frac{n_1 \cdot w_1 + n_2 \cdot w_2}{n_1 \cdot w_1 + n_2 \cdot w_2} \cdot \mu_1 - \frac{n_1 \cdot w_1}{n_1 \cdot w_1 + n_2 \cdot w_2} \cdot \mu_1 - \frac{n_2 \cdot w_2}{n_1 \cdot w_1 + n_2 \cdot w_2} \cdot \mu_2\right)^2$$

$$= \left(\frac{n_2 \cdot w_2}{n_1 \cdot w_1 + n_2 \cdot w_2} \cdot \mu_1 - \frac{n_2 \cdot w_2}{n_1 \cdot w_1 + n_2 \cdot w_2} \cdot \mu_2\right)^2$$

$$= \left(\frac{n_2 \cdot w_2}{n_1 \cdot w_1 + n_2 \cdot w_2} \cdot (\mu_1 - \mu_2)\right)^2$$

$$= \frac{n_2^2 \cdot w_2^2}{(n_1 \cdot w_1 + n_2 \cdot w_2)^2} (\mu_1 - \mu_2)^2$$

In the same way we can rewrite:

$$(\mu_1 - \mu)^2 \qquad = \frac{n_1^2 \cdot w_1^2}{(n_1 \cdot w_1 + n_2 \cdot w_2)^2} (\mu_2 - \mu_1)^2$$

Now, we can use the fact that $(\mu_2 - \mu_1)^2 = (\mu_1 - \mu_2)^2$ to simplify part of Equation (11):

$$w_1 \cdot n_1 \cdot (\mu_1 - \mu)^2 + w_2 \cdot n_2 \cdot (\mu_2 - \mu)^2$$

$$= w_1 \cdot n_1 \cdot \frac{n_2^2 \cdot w_2^2}{(n_1 \cdot w_1 + n_2 \cdot w_2)^2} (\mu_1 - \mu_2)^2 + w_2 \cdot n_2 \cdot \frac{n_1^2 \cdot w_1^2}{(n_1 \cdot w_1 + n_2 \cdot w_2)^2} (\mu_2 - \mu_1)^2$$

$$= \frac{w_1 \cdot n_1 \cdot n_2^2 \cdot w_2^2 + w_2 \cdot n_2 \cdot n_1^2 \cdot w_1^2}{(n_1 \cdot w_1 + n_2 \cdot w_2)^2} (\mu_1 - \mu_2)^2$$

$$= \frac{w_1 \cdot n_1 \cdot w_2 \cdot n_2 \cdot (n_1 \cdot w_1 + n_2 \cdot w_2)}{(n_1 \cdot w_1 + n_2 \cdot w_2)^2} (\mu_1 - \mu_2)^2$$

$$= \frac{w_1 \cdot n_1 \cdot w_2 \cdot n_2}{n_1 \cdot w_1 + n_2 \cdot w_2} (\mu_1 - \mu_2)^2 \qquad (12)$$

Plugging Equation (12) into Equation (11), we find:

$$\sigma = \sqrt{\frac{n}{n-1} \cdot \frac{w_1 \cdot (n_1-1) \cdot \sigma_1^2 + w_1 \cdot n_1 \cdot (\mu_1 - \mu)^2 + w_2 \cdot (n_2-1) \cdot \sigma_2^2 + w_2 \cdot n_2 \cdot (\mu_2 - \mu)^2}{n_1 \cdot w_1 + n_2 \cdot w_2}}$$

$$= \sqrt{\frac{n_1 + n_2}{(n_1 + n_2 - 1) \cdot (n_1 \cdot w_1 + n_2 \cdot w_2)} \cdot \left(w_1 \cdot (n_1 - 1) \cdot \sigma_1^2 + w_2 \cdot (n_2 - 1) \cdot \sigma_2^2 + \frac{w_1 \cdot n_1 \cdot w_2 \cdot n_2}{n_1 \cdot w_1 + n_2 \cdot w_2} (\mu_1 - \mu_2)^2 \right)} \quad (13)$$

Equation (3) and (13) give the weighted mean and standard deviation in terms of the characteristics of the two bins. Filling in the weights $w_i = \sigma_i^{-2}$, we arrive at

$$\mu = \frac{\sigma_1^{-2} \cdot n_1 \cdot \mu_1 + \sigma_2^{-2} \cdot n_2 \cdot \mu_2}{\sigma_1^{-2} \cdot n_1 + \sigma_1^{-2} \cdot n_2} \quad (14)$$

$$\sigma = \sqrt{\frac{n_1 + n_2}{(n_1 + n_2 - 1) \cdot (n_1 \cdot \sigma_1^{-2} + n_2 \cdot \sigma_2^{-2})} \cdot \left(\sigma_1^{-2} \cdot (n_1 - 1) \cdot \sigma_1^2 + \sigma_2^{-2} \cdot (n_2 - 1) \cdot \sigma_2^2 + \frac{\sigma_1^{-2} \cdot n_1 \cdot \sigma_2^{-2} \cdot n_2}{n_1 \cdot \sigma_1^{-2} + n_2 \cdot \sigma_2^{-2}} (\mu_1 - \mu_2)^2 \right)}$$

$$= \sqrt{\frac{n_1 + n_2}{(n_1 + n_2 - 1) \cdot (n_1 \cdot \sigma_1^{-2} + n_2 \cdot \sigma_2^{-2})} \cdot \left(n_1 + n_2 - 2 + \frac{\sigma_1^{-2} \cdot n_1 \cdot \sigma_2^{-2} \cdot n_2}{n_1 \cdot \sigma_1^{-2} + n_2 \cdot \sigma_2^{-2}} (\mu_1 - \mu_2)^2 \right)} \quad (15)$$

6.4 Dataset of more than two bins

Equation (3) gives the formula for a weighted mean of two bins. It can straightforwardly be generalized to hold for any number of bins B_j with means μ_j, standard deviations σ_j, sizes n_j, and weights $w_j = 1/\sigma_j^2$:

$$\mu = \frac{\sum w_j \cdot n_j \cdot \mu_j}{\sum w_j \cdot n_j} = \frac{\sum \sigma_j^{-2} \cdot n_j \cdot \mu_j}{\sum \sigma_j^{-2} \cdot n_j} \quad (16)$$

In the same way, Equation (11) can be generalized to hold for any number of bins B_j, using Equation (16) for the mean μ:

$$\sigma = \sqrt{\frac{\sum n_j}{(\sum n_j) - 1} \cdot \frac{\sum w_j \cdot (n_j - 1) \cdot \sigma_j^2 + w_j \cdot n_j \cdot (\mu_j - \mu)^2}{\sum w_j \cdot n_j}}$$

$$= \sqrt{\frac{\sum n_j}{(\sum n_j) - 1} \cdot \frac{\sum \sigma_j^{-2} \cdot (n_j - 1) \cdot \sigma_j^2 + \sigma_j^{-2} \cdot n_j \cdot (\mu_j - \mu)^2}{\sum \sigma_j^{-2} \cdot n_j}}$$

$$= \sqrt{\frac{\sum n_j}{(\sum n_j)-1} \cdot \frac{\sum (n_j-1) + \sigma_j^{-2} \cdot n_j \cdot (\mu_j-\mu)^2}{\sum \sigma_j^{-2} \cdot n_j}} \tag{17}$$

Note that Equations (13) and (15) for the standard deviation cannot readily be generalized to hold for any number of bins. In case of more than two bins, the weighted mean is first calculated using Equation (16), and then the standard deviation can be calculated using this mean and Equation (17).

References

Kirchner, J. (2006). *Data Analysis Toolkit #12: Weighted averages and their uncertainties.* http://seismo.berkeley.edu/~kirchner/Toolkits/Toolkit_12.pdf

Tatebe, K. (2005). *Combining Multiple Averaged Data Points And Their Errors.* https://docplayer.net/33088897-Combining-multiple-averaged-data-points-and-their-errors.html
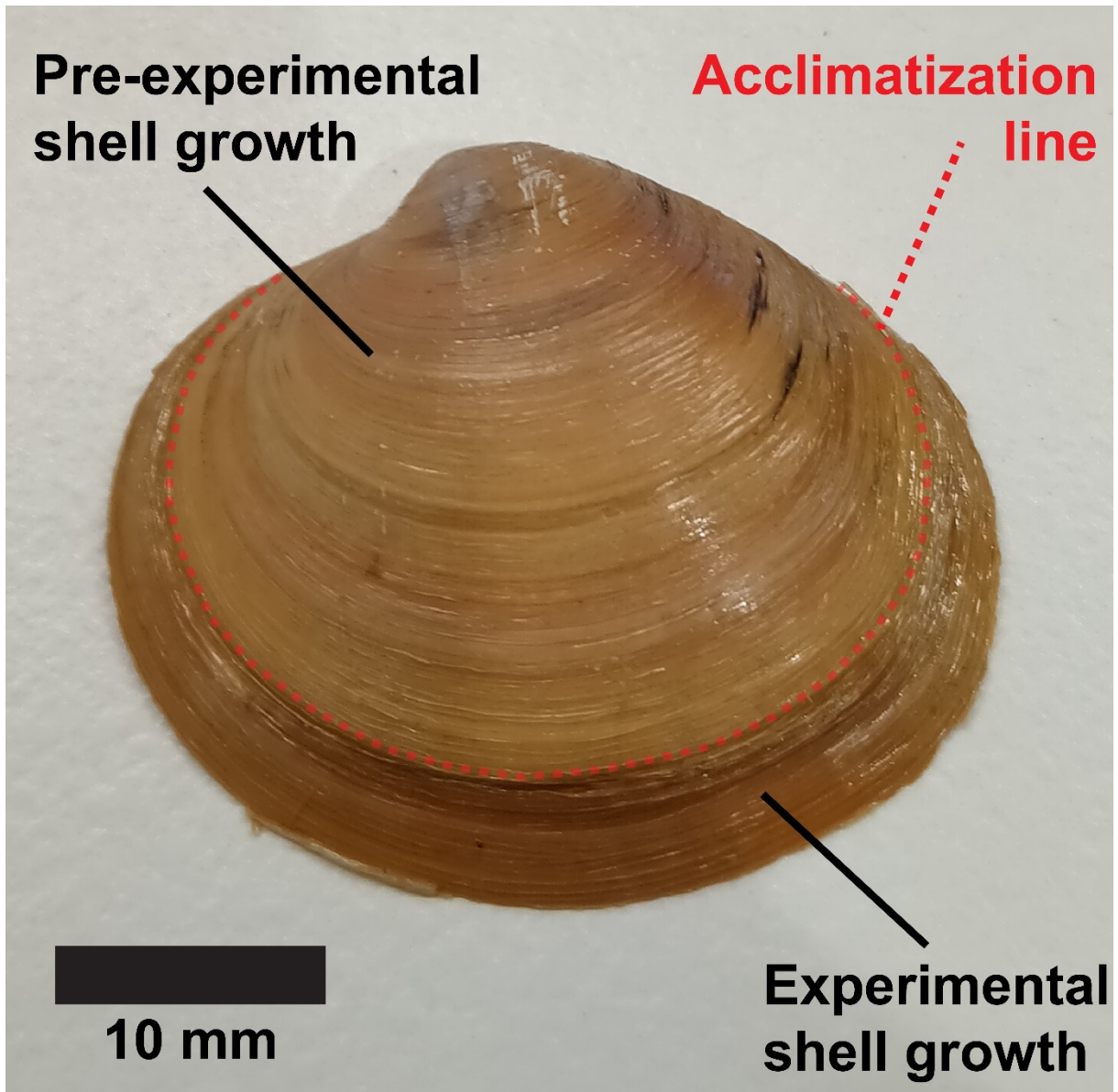
Figure S1. Showing a shell of cultured Arctica islandica with a clearly visible growth mark highlighting transplantation into the culturing conditions.
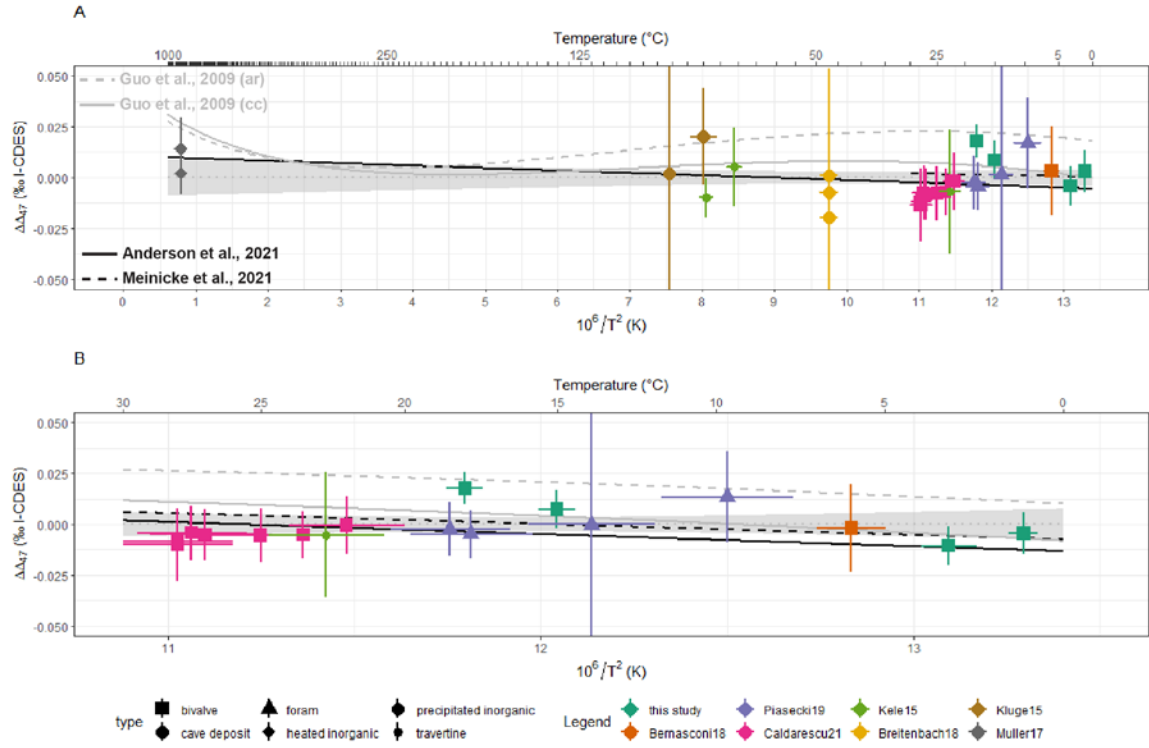
Figure S2. Residuals of aragonite Δ47-temperature relationships. Showing the difference in clumped isotope value (ΔΔ47) between aragonite Δ47 data and the two Δ47-temperature regressions through the aragonite data compilation (see Fig. 2): A) Residuals relative to the York regression through the full dataset. B) Residuals relative to the York regression through only the low-temperature data (<30℃). Results are colored based on the study from which they originated and symbols code for the type of aragonite that was measured (see legend in A, following Fig. 2). Vertical and horizontal bars on symbols indicate uncertainty on Δ47 and formation temperature at the 95% confidence level. Note that some vertical error bars are cropped by the restricted extent of the vertical axis. The solid black line shows the unified clumped isotope calibration by Anderson et al. (2021) while the dashed black line represents the temperature relationship by Meinicke et al. (2020; 2021; only plotted for temperatures below 100℃). Grey solid and dashed lines represent, respectively, the theoretical calcite ("cc") and aragonite ("ar") temperature dependencies from Guo et al. (2009; projected on the I-CDES scale, see section 2.5 in the main text).
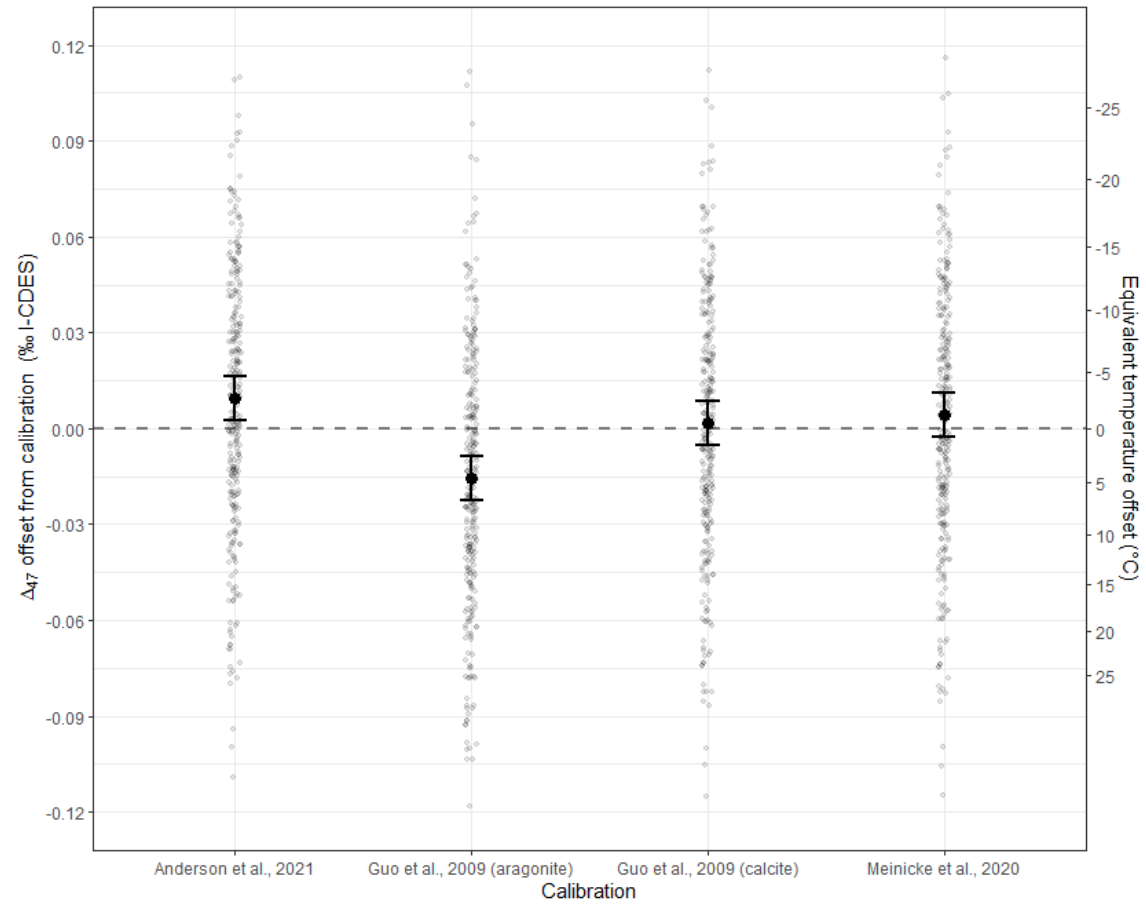
Figure S3. Zoomed out version of Figure 3 in the main text showing residuals of all *A. islandica* aliquots used in this study relative to the four previous clumped isotope temperature calibrations.

Overview of datasets included in aragonite compilation

Sample type	Temperature range ± 1σ	Number of Δ_{47} aliquots	Reference
Precipitated aragonite	80 ± 2°C – 91 ± 0.5°C	11	Kluge et al., 2015
Heated aragonite	850 ±10°C	35	Müller et al., 2017
Cave deposit	47 ± 1°C	16	Breitenbach et al., 2018
Travertine	22.7 ± 1°C – 79.2 ± 1°C	78	Kele et al., 2015
Foraminifera	9.7 ± 1°C – 18.5 ± 1°C	63	Piasecki et al., 2019
Mollusk	6 ± 0.5°C	12	Bernasconi et al., 2018
Mollusk	22 ± 1°C – 28 ± 1°C	165	Caldarescu et al., 2021
Mollusk	1.1 ± 0.2°C – 18 ± 0.3°C	278	This study
TOTAL		8	

Table S1. Overview of aragonite data from previous studies sued for the compilation in this study.